



HAL
open science

Intracellular trafficking and functional monitoring of miRNA delivery in glioblastoma using lipopolyplexes and the miRNA-ON RILES reporter system

Viorel Simion, Elodie Henriet, Viktorija Juric, Ruth Aquino, Claire Loussouarn, Yoan Laurent, Francisco Martin, Patrick Midoux, Emmanuel Garcion, Chantal Pichon, et al.

► To cite this version:

Viorel Simion, Elodie Henriet, Viktorija Juric, Ruth Aquino, Claire Loussouarn, et al.. Intracellular trafficking and functional monitoring of miRNA delivery in glioblastoma using lipopolyplexes and the miRNA-ON RILES reporter system. *Journal of Controlled Release*, 2020, 327, pp.429-443. 10.1016/j.jconrel.2020.08.028 . hal-02959393

HAL Id: hal-02959393

<https://hal.science/hal-02959393>

Submitted on 25 Jun 2021

HAL is a multi-disciplinary open access archive for the deposit and dissemination of scientific research documents, whether they are published or not. The documents may come from teaching and research institutions in France or abroad, or from public or private research centers.

L'archive ouverte pluridisciplinaire **HAL**, est destinée au dépôt et à la diffusion de documents scientifiques de niveau recherche, publiés ou non, émanant des établissements d'enseignement et de recherche français ou étrangers, des laboratoires publics ou privés.



Distributed under a Creative Commons Attribution 4.0 International License

Intracellular trafficking and functional monitoring of miRNA delivery in glioblastoma using lipopolyplexes and the miRNA-ON RILES reporter system

Viorel Simion^{a,*}, Elodie Henriet^a, Viktorija Juric^a, Ruth Aquino^a, Claire Loussouarn^b, Yoan Laurent^a, Francisco Martin^c, Patrick Midoux^a, Emmanuel Garcion^b, Chantal Pichon^a, Patrick Baril^{a,*}

^a Centre de Biophysique Moléculaire, CNRS UPR4301, Université d'Orléans, France

^b CRCINA, INSERM, Université de Nantes, Université d'Angers, Angers, France

^c GENYO, Pfizer/University of Granada/Andalusian Regional Government, Granada, Spain

MicroRNA (miRNA) oligonucleotides therapeutics are potent and attractive drugs for cancer treatment, but the kinetics of their intracellular trafficking, RISC processing and interaction with their mRNA targets in the cells are still not well understood. Moreover, the absence of efficient carriers impairs their translation into the clinic. Here, we compare the kinetics of miRNA-133a activity after transfection of U87MG glioblastoma cells with either a home-made lipopolyplexes (LPRI) or with the RNAiMax transfection reagent. For this purpose, we combined miRNA intracellular trafficking studies by confocal microscopy with our previously described RILES miRNA-ON reporter system subcloned here in a lentivirus expression vector (LentiRILES) for longitudinal analysis of miRNA activity in transfected cells. Using the LentiRILES system, we report significant differences in terms of miRNA delivery kinetics performed by these two transfection reagents. We decipher the mechanisms of miRNA delivery by LPRI and investigate the main steps of miRNA internalization and cytosolic processing. We demonstrate that LPRI preferentially uses caveolae-mediated endocytosis as the main internalization pathway, releases miRNA into the cytosol after the first 3 h of incubation, and addresses the cytosolic miRNAs to P-bodies, while a fraction of miRNAs are exported to the extracellular space through exosomes which were found fully capable to re-transfect the cells. We implanted the LentiRILES cells in the brain of mice and infused the tumours with LPRI.miRNA using the convection-enhanced delivery method. Bioluminescence imaging of the live mice revealed efficient delivery of miRNAs in glioblastoma tumours, attesting successful miRNA uptake, internalization and RISC activation *in vivo*. Overall, our study provides a comprehensive overview of miRNA intracellular trafficking and processing in a glioblastoma context and highlights the potential use of LPRI for miRNA-based therapy.

1. Introduction

MicroRNAs (miRNAs) are a class of endogenous noncoding small RNAs of 18–25 nt that post-transcriptionally regulate the expression of genes in a sequence-specific manner. They bind to mRNA targets, preferentially to the 3'-untranslated region (3'UTR) by a base-pairing mechanism. Since their discovery [1], more than 30,424 mature miRNA products have been annotated in 206 species according to the miRbase Sequence Database [2]. Computational prediction approaches estimate that at least 60% of the human transcriptome can be regulated by miRNAs [3]. Therefore, it is not surprising that miRNA deregulation is a common feature in numerous diseases, including cancer, metabolic or neurological disorders. Preclinical studies have shown that therapeutic modulation of deregulated miRNAs using miRNA-mimics or -inhibitors ameliorates or even reverses the pathological state [4]. De-

spite this tremendous progress, the translation of miRNA-based technologies into the clinic is still limited by their delivery to targeted tissues [5,6]. The delivery barriers include their degradation within the bloodstream, inefficient tumour targeting and endosomal release, immune cells activation and their rapid clearance by the Mononuclear Phagocyte System (MPS) occurring within minutes after their intravenous administration [7].

Local administration of miRNA nanocarriers has the advantage of bypassing most of these physiological barriers and consequently increasing the amount of bioavailable nanocarriers for the targeted organs/cell types. This type of administration is particularly well suited for brain tumours such as glioblastoma (GBM), one of the most lethal types of brain cancer [8]. Glioblastoma propagates locally with rapid invasion of surrounding tissue but without developing metastasis. Therefore, therapeutic intervention on the primary tumour is expected to provide a positive outcome. There are clinically approved, effi-

* Corresponding authors.

E-mail addresses: vsimion@bwh.harvard.edu (V. Simion); patrick.baril@cns-orleans.fr (P. Baril)

cient loco-regional drug delivery methods to bypass the blood brain barrier and to deliver high drug concentrations in specific brain tissues. The convection-enhanced delivery (CED) method is one of these methods and relies on the infusion of drugs into the brain or directly into the tumour mass using intra parenchymal micro catheters connected to a microinjection pump. By applying a constant positive pressure gradient generated by the pump, the therapeutics can diffuse through the interstitial brain fluid resulting in a homogenous and highly concentrated drug distribution in the tumour and/or in the surrounding tissue [9]. Despite all the efforts of cytoreductive surgery in combination with intense chemo-radiotherapy, survival rates for patients with GBM have shown no significant improvement in population statistics [10]. Compared to conventional therapy, miRNA-based therapy delays tumour growth and overcomes chemo-radio resistance [8,11–13]. However, the existing arsenal of miRNA carriers for GBM treatment is currently limited because of the difficulty in complexing a sufficient amount of miRNA cargo in small volumes when considering the loco-regional infusion of brain tumour.

We previously developed nucleic acid carriers called lipopolyplexes and validated their remarkable functionality as mRNA, siRNA and plasmid DNA transfection reagents [14–18]. The miRNA lipopolyplexes (LPri) used in this study are composed of miRNA, a ionizable histidinyllated linear polyethylenimine polymer (His-IPEI) and ionizable liposomes made with O,O-dioleil-N-[3 N-(N-methylimidazolium iodide) propylene] phosphoramidate and the O,O-dioleil-N-histamine phosphoramidate. Both polymer and liposomes contain protonable groups (imidazole) that induce an acid-mediated membrane destabilization of endosomes due to membrane fusion and/or a proton sponge mechanism favouring nucleic acid delivery in the cytosol [14,19–21]. Although this formulation was found previously efficient for siRNA transfection, the exact mechanism by which the siRNA cargo is distributed into the cytosol and how it is processed by the RNAi machinery in order to be functional was not reported. Several studies have explored the intracellular trafficking of various forms of RNAi oligonucleotides and their release to the cytosol [22–26]. It is now well established that most of the internalization routes of nucleic acid carriers converge to early and/or late endosomal vesicles where they must escape into the cytosol to prevent their trafficking and degradation [25]. Nevertheless, deciphering the underlying mechanisms of cellular uptake, internalization and RNAi processing remains still a challenging process. It is known that the size and the shape of the lipid and/or polymer composition of nanocarriers impact on the route of internalization and intracellular delivery of the RNAi cargo. Furthermore, different cell types can use different endocytosis pathways to internalize the same carrier [23,27–29]. The complexity increases even further when considering the subcellular sites where the RISC machinery processes the miRNAs to become functional. Early studies have reported that a significant fraction of endogenous miRNAs is transported to distinct cytoplasmic foci known as P-bodies, together with their targeted mRNAs and Argonaute 2 [30,31]. It was proposed that miRNAs and RNAi proteins guide their target mRNAs to these P-body condensates for translational inhibition and mRNA degradation [32–34]. It was thereafter demonstrated that microscopically visible P-bodies do not seem to be required for efficient RNAi silencing activity although the silencing of some specific P-body proteins impairs mammalian RNAi activity [30,35]. While it is now almost admitted that P-bodies are the consequence and not the cause of mRNA silencing [36], the exact role of P-bodies in RNAi processing is still under debate.

Since it is difficult to predict the intracellular trafficking of a miRNA nanocarrier in cells and because there is still no clear picture of the sites of miRNA processing in the cytosol after internalization, here, we combined intracellular trafficking studies of miRNA by confocal microscopy with our previously described RILES miRNA-ON reporter system [37–39]. We subcloned the RILES system in lentivirus expression plasmids (LentiRILES) to stably maintain the expression of this miR-

ON sensor in U87MG glioblastoma cells. We established the kinetic of miRNA activity upon delivery in U87MG LentiRILES cells and report qualitative, quantitative and spatial information on the fate of miRNA mimics in cells after transfection. We describe the main steps of the miRNA intracellular trafficking, endosomal release, cytosolic storage into P-bodies and extracellular export *via* exosomes containing functional miRNAs. We evaluate the potential of our LPri as a miRNA glioblastoma nanocarrier by CED infusion of U87MG LentiRILES brain tumours and bioluminescence imaging. Overall, our study highlights the promising potential of LPri for miRNA therapy of GBM.

2. Materials and methods

2.1. LPri preparation and loading with synthetic miRNAs

The synthetic miRNAs used in this study were from ThermoFisher (mirVana miRNA Mimics). His-IPEI (PTG1; Mw = 34.5 kDa) was purchased from Polytheragene (Evry, France). O,O-dioleil-N-[3 N-(N-methylimidazolium iodide) propylene] phosphoramidate (KLN25; Mw = 787 Da) and O,O-dioleil-N-histamine phosphoramidate (MM27; Mw = 692 Da) were kindly given by Prof. Paul Alain Jaffres and Dr. Mathieu Berchel (UBO, Brest, France) [40,41]. LIP100 liposomes (KLN25/MM27, 1/1 M ratio) were prepared at 5.4 mM in 10 mM Hepes buffer, pH 7.4 by the film hydration method as described [42]. For *in vitro* transfection, LPri lipopolyplexes were prepared as previously described [14], by first mixing 2.1 µg His-IPEI (4.2 µL of a stock solution at 0.5 mg/ml) with 0.7 µg miRNA mimics (10 µL of a stock solution at 5 µM) in 14.2 µL of 10 mM Hepes, pH 7.4 to reach an optimal miRNA/polymer weight ratio of 1/3. After 5 s vortex, the solution was kept 30 min at 20 °C. The amount of LIP 100 used to encapsulate the His-IPEI.miRNA polyplexes was calculated according to the molecular weight of synthetic miRNA (23 nt, Mw = 15,180 g/mol) and their negative charges to generate an optimal miRNA/lipid charge ratio of 1/2. Thus, 200 µL (3.6 µg) of LIP100 liposomes 10 mM Hepes, pH 7.4 (8.4 µL of a stock solution at 0.54 mM) were mixed with the polyplexes and kept 15 min at 20 °C. The LPri solution was adjusted to 1 mL with serum-free RPMI medium and 0.5 mL were added to the cells in 24-well plates. For *in vivo* transfection, LPri were prepared by first mixing 201 µg His-IPEI (8.4 µL of a stock solution at 25 mg/ml) with 67 µg miRNA mimics (10 µL of a stock solution at 500 µM) in 28.4 µL of 10 mM Hepes, pH 7.4 (miRNA/polymer weight ratio of 1/3). After 5 s vortex, the solution was kept 30 min at 20 °C. Then, 200 µL (345 µg) of LIP100 liposomes 10 mM Hepes, pH 7.4 (147 µL of a stock solution at 5.4 mM) were mixed with the polyplexes (miRNA/lipid charge ratio of 1/2) and kept 15 min at 20 °C. Then, 7 µL of this LPri solution containing 2 µg of miRNA-133a was infused by CED at a speed of 0.5 µg/µL into the brain of mice.

2.2. Plasmids

For the pRab5-EGFP and pRab7-EGFP plasmids, the C-terminus of Rab5 and Rab7 genes was fused with cDNA expressing enhanced green fluorescent protein (EGFP) in the pEGFP-N1 vector from Clontech (Takara Bio Europe) under the cytomegalovirus (CMV) promoter, and were a kind gift from Dr. A. Galmiche (University of Würzburg, Würzburg, Germany). pCav1-GFP was a gift from Ari Helenius (Addgene plasmid # 14433). This plasmid encoded for caveolin1 gene fused with GFP gene under the cytomegalovirus (CMV) promoter. pLAMP1-mGFP was a gift from Esteban Dell'Angelica (Addgene plasmid # 34831), pT7-EGFP-C1-HsDCP1a was a gift from Elisa Izaurrealde (Addgene plasmid # 25030), pmyc-GFP-TNRC6A (GW182) was a gift from Kumiko UiTei (Addgene plasmid # 41999), pCMV-RFP-RCK/p54 (DDX6) was a gift from Dominique Weill (Institut de Biologie de Paris-Seine, Paris, France). Supercoiled DNA was isolated from *Escherichia coli* DH5a super competent bacteria (Invitrogen ThermoFisher Scien-

tific) by alkaline lysis and purification with Qiagen Mega Kit Endotoxin free Plasmid (Qiagen).

2.3. Agarose gel shift assay

The miRNA mimics binding capacity of His-IPEI polyplexes, Lip100 lipoplexes and LPri lipopolyplexes was evaluated using the agarose gel retardation assay as previously described [14]. Electrostatic complexes with different molar ratios or charge were obtained by mixing miRNA mimics with appropriate quantities of His-IPEI polymer and Lip100 liposomes, together or separately, in 10 mM Hepes solution pH 7.6. Thirty minutes after mixing, the resulting colloidal solutions were loaded in a 1% agarose gel, and electrophoresis experiments were carried out at 90 V, for 90 min, in TAE buffer solution. The migration of miRNA mimics free or in complexed states was visualized under UV light, after gel staining with ethidium bromide.

2.4. Tissue culture

U87MG human glioblastoma cells were from ATCC (American Type Culture Collection) and were cultured in Dulbecco's modified Eagle's medium (DMEM) supplemented with 10% fetal calf serum (FCS) and Penicillin (100 U/mL) and Streptomycin (100 µg/mL) antibiotics at 37 °C with 5% CO₂. The NG2 glial progenitor cells (a gift from Severine Morriset, CBM, CNRS UPR4301) were cultured in Neurobasal medium with B27 supplements (NBM/B27) (Invitrogen) containing 10 ng/ml PDGFAA (Roche). For experiments, the cells were seeded in 6- or 24-well plates at a density of 1.5E+4 or 3.5E+3 cells per well respectively and grown overnight before transfection. Cells were mycoplasma-free as evidenced by the MycoAlert Mycoplasma Detection Kit (Lonza, France).

2.5. LentiRILES/133 T stable cell lines production

The lentiviral plasmids containing the RILES constructs were provided by Francisco Martin (GENYO, Pfizer/University of Granada, PTS Granada, Spain) and derived from a previous publication [43]. To place the Tet R transcriptional repressor under control of miRNAs, miRNA targeting sequences were prepared as previously described [37–39] and subcloned downstream of the Wpre, Woodchuck hepatitis virus post-transcriptional regulatory element. The sequence of the miR 133 T cassette used to monitor the expression of miRNA 133a is fully available upon request. The method to produce the LentiRILES particles is based on a standardized procedure [43]. Briefly described, the 293 T cells were plated in a 75 cm² flask and transfected the following day with the LentiRILES, packaging, and envelope plasmids at a plasmid proportion of 3:2:1 respectively using the His-IPEI polymer. After 72 h, the medium containing viral particles was collected, centrifuged, filtered through a 0.45 µm sterile filter and stored at –80 °C until further use. Titration of the lentivirus batches was performed according to the method described here [43]. The production of LentiRILES-stable cell lines was performed by the transduction of U87MG cells with LentiRILES viral particles at different M.O.I (multiplicity of infection) in the presence of 10 µg/mL of polybrene (Sigma). Screening of the most responsive LentiRILES/133 T cell line was performed by transfection of cells with miRNA-133a and miRNA control mimics complexed with the RNAiMax transfection reagent according to the manufacturer's recommendations (Thermo Fisher Scientific). Bioluminescence signals emitted from the LentiRILES/133 T cells were quantified in a 96-well plate using an IVIS Lumina II imaging scanner (Perkin Elmer, USA) or from cell lysate using an LB 940 Mithras spectrophotometer (Berthold, France) and normalized to protein content (RLU/mg protein) as previously described [37–39].

2.6. miRNA mimics, siRNAs and plasmids transfections

For intracellular trafficking studies, the cells were first seeded in 6-well plates and after 24 h transfected with 1 µg of the indicated plasmids encoding EGFP- or RFP-fused genes using Lipofectamine 2000 (Invitrogen Thermo Fisher Scientific) according to the manufacturer's protocol. Transfected cells were then seeded in 24-well plates with glass coverslips at the bottom of the wells (2.5E + 4 cells/cm²) and after 24 h the cells were transfected with LPri complexed with 350 ng (50 nM) of miRNA-133a mimics labelled with Cyanine 3 (Cy-3)- or fluorescein (FL). The miRNA mimics were labelled using the Label IT nucleic acid labelling kit (Mirus Bio, USA), according to the manufacturer's protocol. Briefly, 20 µg miRNA mimics were incubated with 20 µL of Mirus miRNA labelling kit, 25 µL of 10 × Buffer and 50 µL of nuclease-free water. After incubation for two hours at 37 °C, 3.5 µL Glicogen, 25 µL of 5 M Sodium Chloride and 750 µL of 75% Ethanol were added, mixed and further incubated at –20 °C overnight. The labelled miRNAs were pelleted by centrifugation at 12.000 g and washed with 75% Ethanol, dried and resuspended in TE buffer. For endosomal escape studies, the miRNA mimics were combined with FITC-labelled phosphorothioate oligonucleotides (FITC-5'-ACTACGACCTACGTGAC-3') [22] at a 1:1 M ratio and complexed by the LPri and further transfected as described above. Fluorescent microscopy images were taken at the indicated time points by epifluorescence microscopy. For siRNA silencing studies, the U87MG LentiRILES/133 T cells were seeded in 24-well plates overnight, then transfected with Dharmacon ON-TARGET siRNAs (Horizon Discovery, USA) for AGO-2, DCP1a, DDX6 (RCK/p54) and GW-182 (TNR-C6A) using the Lipofectamine RNAiMax as transfection reagent and according to manufacturer recommendations (Thermo Fisher Scientific). Then 24 h later, the cells were transfected with the LPri.miRNA-133a or LPri.miRNA CTL mimics.

2.7. Confocal laser scanning microscopy and colocalization quantification

Cells were fixed in 3% paraformaldehyde (PFA) in PBS solution at room temperature for 10 min and excess paraformaldehyde was removed with 3 washes of 5 min in phosphate-buffered saline (PBS). For immunocytochemistry the coverslips were incubated overnight at 4 °C with AGO-2 antibody (1:200, Abcam, France), then washed and incubated for 1 h with anti-mouse Alexa-485 antibody (Life Technologies Thermo Fisher Scientific). Then, the coverslips were mounted in Vectashield medium for fluorescence (H-100, Vector Laboratories, USA). Confocal microscopy was performed using a Zeiss LSM 510 confocal laser scanning microscope with an apochromat 63 × /1.4 oil differential interference contrast (DIC) objective (Carl Zeiss, USA). Each coloured image was split into respective red and green channels and ImageJ software was used to quantify the cell-associated fluorescence, using the JACoP (Just Another Co-localization Plugin) plug-in. The comparative degree of co-localization was calculated as the fraction of Cy3-miRNA signals (red) colocalizing with signals from intracellular vesicles/condensates (green) and expressed as Mander's R (*Mr*) colocalization coefficients. Quantification results were obtained by analysing 15–30 images (different cells) for every time point, from three independent experiments.

2.8. Quantitative real-time PCR

The procedure for quantitative real-time PCR analysis was exactly the same as described previously [37,38] except that the primers used for detection of miRNA were purchased from Qiagen.

2.9. Exosome purification and characterization

U87MG cells were transfected with LPri/miRNA-133a or LPri/miRNA CTL for 8 h as described above and the medium was replaced with serum-free medium. After 3 days of incubation, supernatants from $5 \times 75 \text{ cm}^2$ tissue culture flasks for each transfection condition were collected, pooled, and the exosomes were purified as previously described [44]. Briefly, the medium was serially centrifuged at 4°C for 10 min at 480 g, 10 min at 2000 g, 30 min 5000 g and then ultracentrifuged for 1 h at 100000 g (Beckman rotor Ti45). The pellet was resuspended in PBS and ultracentrifuged for another 1 h at 100000 g 4°C and finally resuspended in 100 μL PBS before being stored at -80°C . Exosome quantification was estimated according to their protein content using a standard BCA protein assay. For exosome biochemical characterization, 10 μg of equivalent protein content of exosome samples was solubilized in Laemmli buffer, resolved on 8% SDS-PAGE gel and immunoblotted using Alix (clone MAI-83977, Invitrogen Thermo Fisher Scientific), GM130 (clone D6B1, Cell Signaling, USA) and TSG101 (clone EXOAB-TSG101-1, System Biosciences, USA) antibodies. For detection of miRNA in exosome, 300 μL of 1/100 dilution of exosome samples were treated using recommendations from the Nucleospin miRNA plasma kit (Macherey-Nagel, France). After total RNA extraction, 100 ng of tRNA were reverse-transcribed using the miScript II RT kit (Qiagen) and then miRNAs were quantified using the miScript SYber green PCR kit (Qiagen) with specific primers from Qiagen. Primers specific to miRNA-23a and -21.5p were used as miRNA-housekeeping genes to normalize the relative expression of miRNA-133a detected in exosome from LPri.miRNA 133a and LPri.miRNA CTL transfected cells.

2.10. Nanosizer, Atomic force microscopy (AFM) and Transmission electron microscopy (TEM) studies

The size and ζ potential of LPri.miRNA lipopolyplexes and the exosomes were measured in 10 mM Hepes buffer, pH 7.4 using the SZ-100 Partica Nanosizer Analyser (Horiba Scientific, Japan) according to a routine procedure used in our laboratory [15,45]. For topographical investigations, 5 μL of LPri.miRNA complexes were added on a mica disc, dehydrated and analysed by atomic force microscopy. The AFM scans were performed in AC mode with a 5 V amplitude bias applied between the tip and the sample at 3 kHz. TEM studies were performed at the University of Orléans and employed to visualize the size and shape of exosomes collected from U87MG cells transfected with LPri.miRNA-133a and LPri.miRNA CTL according to the procedure described here [46]. Briefly described, 5 μL of exosome suspension was loaded on a carbon coated copper grid negatively charged using UV light. After 5 min of decantation, the solution was adsorbed with filter paper and exosomes stacked on the carbon layer were negatively stained for 15 s with 5 μL of 2% uranyl acetate solution prepared in distilled water. After drying, the sample was observed using a TEM CM20 (Philips, Netherlands) operating at 160 kV and equipped with a LaB6 filament. Electron micrographs were captured using an AMT XR80 digital camera (Advanced Microscopy Techniques, USA).

2.11. In vivo studies

All mouse experiments were carried out in strict accordance with the rules of the French Ministry of Agriculture and the European Communities Council Directive (86/609/EEC). The experimental protocol used in this study was approved by the "Pays de la Loire" Ethics Committee of Animal Experiments (Permit No. CEEA. 2012.60; Authorization n°A 49-2012-04). Female CB-17/Icr-Prkdc scid/Rj mice (7 weeks old, Janvier Labs, France) were maintained in pathogen-free conditions with controlled temperature ($20\text{--}22^\circ\text{C}$), humidity ($50\text{--}70\%$),

light (12 h light/dark cycles) and housed with unlimited access to food and water. The U87MG LentiRILES/133 T cells were transduced with pre-made Renilla luciferase viral particles (R-Luc, OriGene EU, France) at MOI (multiplicity of infection) of 10 according to the procedure described above. Thereafter the dual LentiRILES/133 T reporter cell line was implanted in the brain of mice by stereotactic surgery using a stereotaxic frame (lab standard™ stereotaxic, USA) as described previously [47]. Seven μL of tumour cells (7×10^6 cells/mL) were inoculated manually in the right striatum (anterior -0.5 mm, lateral 2.5 mm, depth -3.5 mm according to the Bregma) using a 10 μL syringe (Hamilton® glass syringe 700 series RN, Hamilton, USA) connected to a 26-G needle (Hamilton®). After 12 days, glioblastoma tumour development was confirmed by MRI imaging as described previously [47] and then animals were randomly assigned to 2 groups. The miRNA (2 μg) were formulated with LPri as described above to reach a 7 μL final volume solution prepared in 5% glucose and 60 mM NaCl. The LPri.miRNA were thereafter infused into solid tumours by CED. For this second infusion, syringes were equipped with a 32-G needle connected to the Harvard apparatus Pump but injections were carried out automatically at a constant flow rate of 0.5 $\mu\text{L}/\text{min}$ over a period of time of 18 min. The mice were then monitored daily for mobility, grooming and weight. Three days after CED infusion of tumour with the LPri.miRNA, the Firefly luciferase substrate (150 μL of luciferin solution at 20 mg/ml, Promega) was intraperitoneally injected to the mice before scanning the animals 10 min later using an IVIS bioluminescence imaging scanner (Perkin Elmer). The mice were thereafter returned to the cage for 6 h and then the Renilla Luciferase substrate (100 μL of Coelenterazine at 35 mg/ml, Perkin Elmer) was injected intravenously to the mice before scanning the animals 2 min later using the IVIS bioluminescence imaging scanner. Image acquisition and treatment were performed from regions of interest (ROI) drawn manually and quantified as photons/second/pixel/sr using the living Image Software (PerkinElmer) and as previously described [37–39].

2.12. Statistical analysis

Results throughout the study are expressed as mean \pm S.E.M. Prism GraphPad software (V.7.0a) was used for statistical analysis using unpaired two-tailed Student's *t*-test or one-way ANOVA with Bonferroni correction for multiple comparisons. A probability of $p < 0.05$ was considered statistically significant. ns, not significant; * $p < 0.05$; ** $p < 0.01$; *** $p < 0.001$; **** $p < 0.0001$.

3. Results

3.1. Kinetics of the miRNA transfection monitored by LentiRILES system

In previous studies, we engineered a genetic switch expression system called RILES (RNAi-Inducible Luciferase Expression system) to monitor the activity of endogenously expressed miRNAs upon transient transfection of cells or tissues [37–39]. In this study, we subcloned the RILES system in lentivirus expression plasmids to stably maintain the expression of this miR-ON sensor in fast-dividing biological systems such as cancer cells. We replaced the Cumate-inducible gene expression system (Cumate operon) of the RILES with the tetracycline-inducible gene expression system (tetracycline operon) in the Tet R configuration. Similar to the Cumate operon, the Tet R tetracycline operon works through the binding of a transcriptional Tet R repressor protein on operator sequences (Tet O) to regulate transgene expression [48].

The tetracycline operon was placed under control of miRNA-133a by subcloning 4 complementary block sequences of this miRNA (miR T cassette) in the 3'UTR region of the transcriptional repressor Tet R. The choice of miRNA-133a was based on experimental evidence that this miRNA is barely expressed in cancer cell lines such as U87MG (Fig. 1A). Consequently, once delivered in cells, this miRNA is not expected to interfere with the endogenous machinery of U87MG cells. Fig. 1

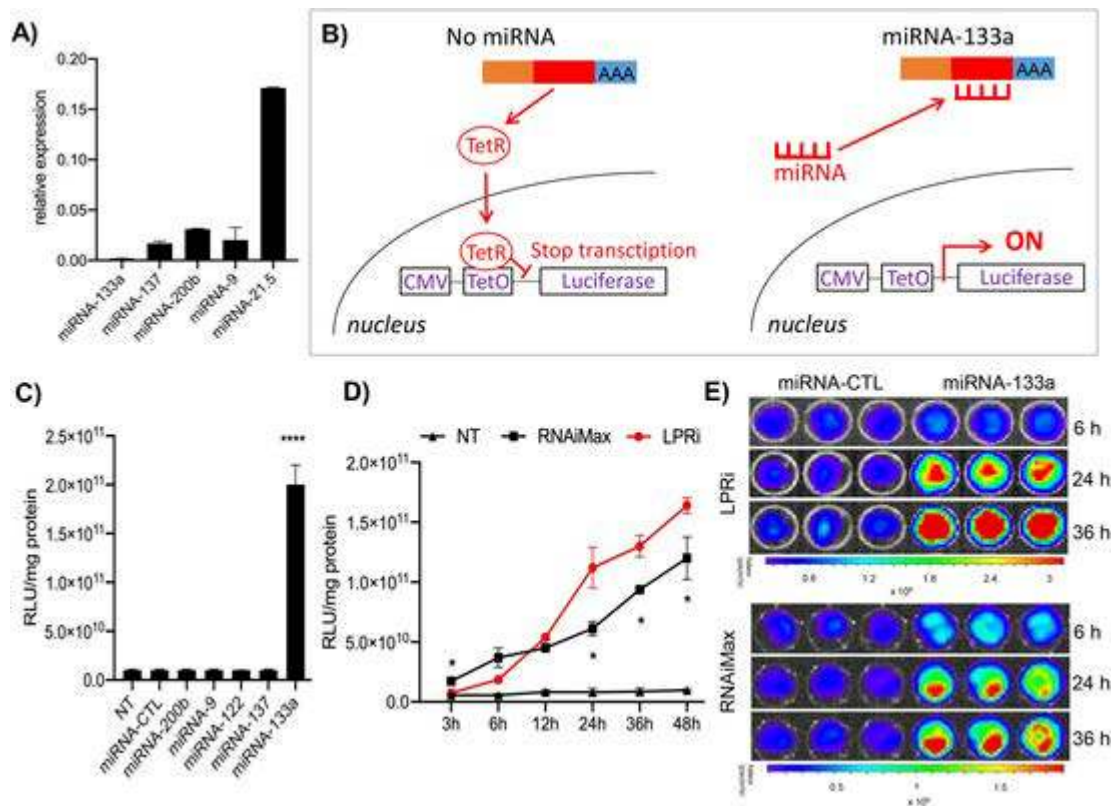


Fig. 1. Design, validation and specificity of the U87MG LentiRILES/133 T miRNA-ON reporter cell line to miRNA-133a. **A)** Relative expression of several miRNAs, including miRNA-133a, in the U87 MG cell line detected by qRT-PCR ($n = 4$). **B)** Schematic representation of LentiRILES/133 T mechanism of action placed under control of miRNA-133a. In the absence of miRNA-133a (*left panel*), the Tet R transcriptional repressor binds to the Tet O operator and switches OFF the expression of the Luciferase reporter gene. In contrast, in the presence of miRNA-133a (*right panel*), the expression of the transcriptional repressor Tet R is suppressed, resulting in the expression of the Luciferase reporter gene and emission of bioluminescence signals in cells. **C)** Validation of the LentiRILES/133 T specificity and sensitivity after transfection of the U87MG LentiRILES/133 T cells with miRNA-133a or non-relevant miRNAs, including control miRNA (miRNA CTL) ($n = 5$). Kinetics of luciferase expression detected in the U87MG LentiRILES/133 T cells after transfection with miRNA-133a using either the RNAiMax or the LPRi lipopolyplexes quantified in the whole cell lysates. The number of relative light units (RLU) was expressed per mg of protein (**D**) or in real time using an IVIS Lumina imaging scanner (**E**); one representative experiment performed 3 times. For all panels, values are mean \pm SEM. * $p < 0.05$, ** $p < 0.01$; *** $p < 0.001$; **** $p < 0.0001$.

B represents the working principle of the RILES-miRNA monitoring system. When transfected in cells, miRNA-133a will bind to the miR T cassette resulting in the activation of the RISC machinery and consequently transcriptional repression of the Tet R mRNA and protein. Therefore, in the absence of the Tet R bound on the Tet O operator, the inducible promoter driving the firefly luciferase (F-Luc) expression will be switched-ON, resulting in the emission of bioluminescence signals in cells (Fig. 1B). To subclone the RILES in a Lentivirus expression system, we took advantage of the dual Tet R-based lentiviral system developed by Benabdellah et al. [43] in which the Tet R and Tet O regulatory molecules were expressed separately in two different lentiviral vectors. After optimization, we found that a 2/1 MOI ratio of Tet R/Tet O lentiviral particles was the best ratio to produce an optimal responsive U87MG RILES stable cell line to miRNA-133a. This stable cell line was denoted U87MG LentiRILES/133 T.

We first evaluated the sensitivity and specificity of U87MG LentiRILES/133T to miRNA-133a. We demonstrated that the transfection of miRNA-133a in U87MG LentiRILES/133T cells resulted in induction by 9-fold of the luciferase expression compared to cells transfected with a miRNA control mimic. Similarly, the transfection of irrelevant miRNAs such as miRNA-200b, -9, -122, -137 did not induce significant luciferase expression (Fig. 1C). We then evaluated the relative toxicity of the LPRi to the U87MG cells and, as representative glial cell population of the mature central nervous system, the NG2 cells [49]. Data in Supplementary Fig. S1, indicated that transfection of these two cell types with the LPRi did not induce any significant cellular toxicity in con-

trast to the RNAiMAX. These two transfection reagents were found however equally capable to transfect the NG2 cells.

We then established the kinetic of miRNA-133a activity in the U87MG LentiRILES/133T cells transfected with either the LPRi or with the golden standard miRNA transfection reagent, Lipofectamine RNAiMax. As shown in Fig. 1D, the kinetics of miRNA-133a activity detected in cells after transfection were very distinct: RNAiMax induced a 2-fold increase in luciferase activity as early as 3 h post-incubation, followed by a constant increase during the next 48 h. In contrast, after 3 h the activity of luciferase detected in cells transfected with the LPRi was low and not statistically significant compared to the luciferase activity detected in non-transfected cells. However, at later time points, from 6 to 12 h, the luciferase activity in cells transfected with the LPRi increased and was found to be similar to the luciferase activity detected in cells transfected with the RNAiMax. Interestingly, above this time point and for the following 36 h, the luciferase activity of LPRi-transfected cells increased gradually and was significantly higher than the luciferase activity detected in cells transfected with the RNAiMax (Fig. 1D, E). These results indicate that at early time points the process of miRNA-133a delivery in cells is delayed when the LPRi was used as transfection reagent, while at later points it is accelerated as compared to RNAiMax. Importantly, similar results were obtained when the luciferase activity in U87MG LentiRILES/133T was monitored in real-time, in live cells using a bioluminescence imaging scanner, a prerequisite for *in vivo* live imaging of miRNA expression in small animal models (Fig. 1E).

3.2. Physicochemical characterization of the LPRi.miRNA-133a complexes

As we found that the kinetics of miRNA-133a delivery was different when comparing LPRi to RNAiMAX, we then attempted to decipher the underlying process of our LPRi transfection reagent. We first characterized the miRNA-133a mimic after formulation with LPRi. Since the LPRi formulation is a ternary complex composed of His-IPEI as polymer and LIP 100 as liposomes and miRNAs as nucleic acids (Fig. 2A), we evaluated the miRNA complexation efficacy of each component taken individually by a gel shift assay. The results in Fig. 2B indicate that the His-IPEI complexed the miRNA almost totally at a miRNA/polymer weight ratio of 1/6. The size of the generated polyplexes exhibited an average hydrodynamic size of 149.4 nm with a ζ potential of +8.4 mV and a polydispersity index of 0.27 (Fig. 2C). The miRNA was also entirely complexed with LIP100 liposomes at a miRNA/liposome charge ratio of 1/4. The size of the generated lipoplexes exhibited an average hydrodynamic size of 180.9 nm with a ζ potential of +17.2 mV and a polydispersity index of 0.18 (Fig. 2C). The lipopolyplexes were then prepared by first complexation of the miRNA with the His-IPEI polymer to create uniform polyplexes and then incubated with the LIP 100 liposomes to encapsulate them. Fig. 2A shows that the miRNA was totally complexed with His-IPEI at a ratio of 1/3 and thereafter with LIP 100 liposomes at a charge ratio of 1/2. The size of the generated lipopolyplexes exhibited an average hydrodynamic size of 117.9 nm with a ζ potential of +49.1 mV and a polydispersity index of 0.31. The significant reduction in size of the lipopolyplexes observed after addition of the LIP 100 liposome supported the encapsulation of polyplexes in liposomes as previously documented with siRNA [14]. Furthermore, Atomic Force Microscopy (AFM) in Fig. 2D revealed a compacted, circular-like nano-object similar to lipopolyplexes previously characterized [15–17,50]. We finally evaluated the stability of the LPRi lipopolyplexes when incubated for 1 h at 37 °C in 0.9% NaCl as physiological buffer and at pH 4. Results from a gel shift assay demonstrated that the LPRi.miRNA lipopolyplexes are stable nanoparticles. Neither the pH, nor the physiological buffer reversed the complexation of miRNAs by the LPRi. No free-miRNA bands were detected on agarose gel in these conditions including condition in which the LPRi.miRNA nanoparticles were exposed for 1 h at pH 4 (Supplementary Fig. S2).

3.3. Endosome escape of LPRi and Lipofectamine RNAiMax

We then focused our investigations on the endosomal escape capacity of the LPRi and RNAiMAX, a stringent limiting step for nucleic acid delivery [22,24]. It was previously documented that oligodeoxynucleotides (ODN) passively accumulate in the nucleus, once they reach the cytosol [21,51,52]. We took advantage of this feature to monitor the endosomal escape step controlled by LPRi and RNAiMax. Thus, equimolar mixtures of Cy5-miRNA-133a mimics and FITC-ODN were complexed with either LPRi or RNAiMax. We first ensured that most of the lipopolyplexes ($98 \pm 1.1\%$) were both Cy5- and FITC-positive by quantifying, by confocal microscopy, the percentage of red dots colocalizing with the green dots and *vice-versa*. This study was performed *in vitro*, after loading the LPRi.miRNA.ODN on a microscope slide (Supplementary Fig. S4A). U87MG cells were transfected and fluorescence microscopy analysis was used to detect the presence of FITC signals in nuclei (Fig. 3A and Supplementary Fig. S4B). Kinetics results indicated that 27% of the cells incubated with RNAiMax had FITC-positive nuclei after 3 h incubation while almost no FITC fluorescence signal was detectable in the nuclei of cells incubated with LPRi (Fig. 3C). After 6 h incubation, 38% of the cells incubated with RNAiMax had FITC-positive nuclei signals against only 17% of cells transfected with LPRi. However, from 10 to 14 h, the percentage of fluorescent nuclei in LPRi transfected cells increased dramatically from 45 up to 89%, while the percentage of positive fluorescent nuclei of RNAiMax transfected cells increased only mildly (Fig. 3C).

3.4. miRNA endocytosis and intracellular trafficking

We next sought to determine the nature of the endocytosis pathways used by U87MG cells to internalize the LPRi.miRNA-133a. We first assessed the concentrations of Chlorpromazine (6 μ M), Filipin (0.75 μ M), Genistein (7.5 μ M), cytochalasin D (0.12 μ M) that did not induce toxicity [53] (Supplementary Fig. S3A). Then we evaluated the impact of these inhibitors on the LPRi.miRNA-133a transfection efficiency as estimated by luciferase activity detected in the U87MG LentiRILES/133 T. As shown in Fig. 4A, the luciferase activity was significantly reduced when the cells were pre-incubated for 2 h with Fil-

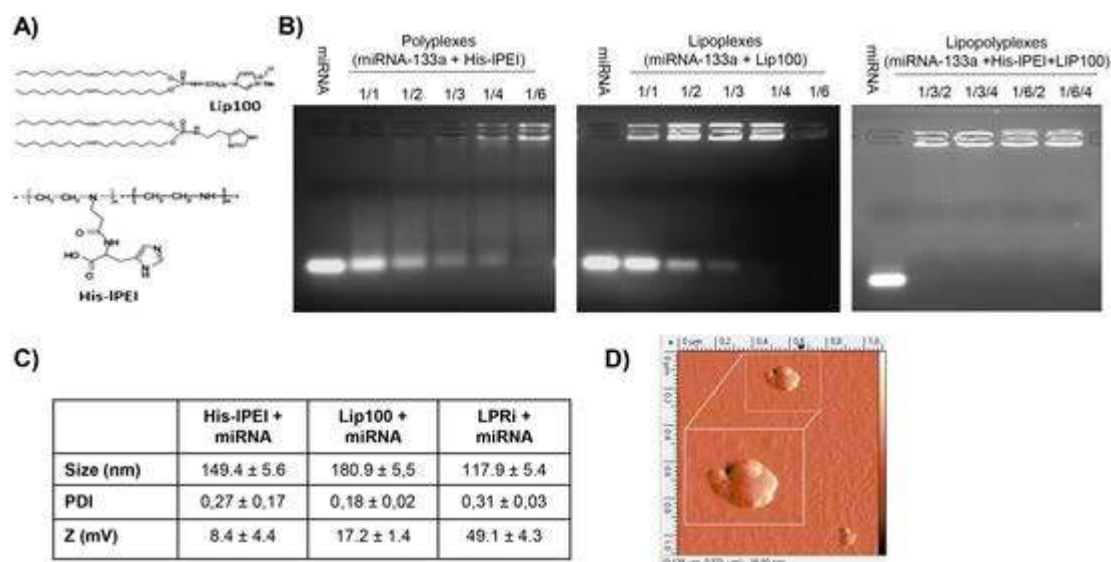


Fig. 2. Physicochemical characterization of LPRi.miRNA-133a. A) Chemical formula of LPRi components: Lip100 liposomes formed using the lipids O,O-dioleoyl-N-[3 N-(N-methylimidazolium iodide) propylene]phosphoramidate (cationic lipid) and the O,O-dioleoyl-N-histamine phosphoramidate (MM27), and the histidinylated linear polyethylene imine (His-IPEI) polymer; B) Agarose gel shift migration of polyplexes (miRNA mimics + His-IPEI), lipoplexes (miRNA mimics + Lip100 liposomes) and LPRi lipopolyplexes (miRNA mimics + His-IPEI + LIP100) showing efficient miRNA complexation of LPRi. C) Nanosizer determination of size, polydispersity index (PDI) and Zeta (Z) potential (mV) of His-IPEI/miRNA, Lip100/miRNA and LPRi/miRNA complexes. D) Atomic force microscopy (AFM) of LPRi/miRNA complexes. The figures are representative of one experiment repeated 3 times.

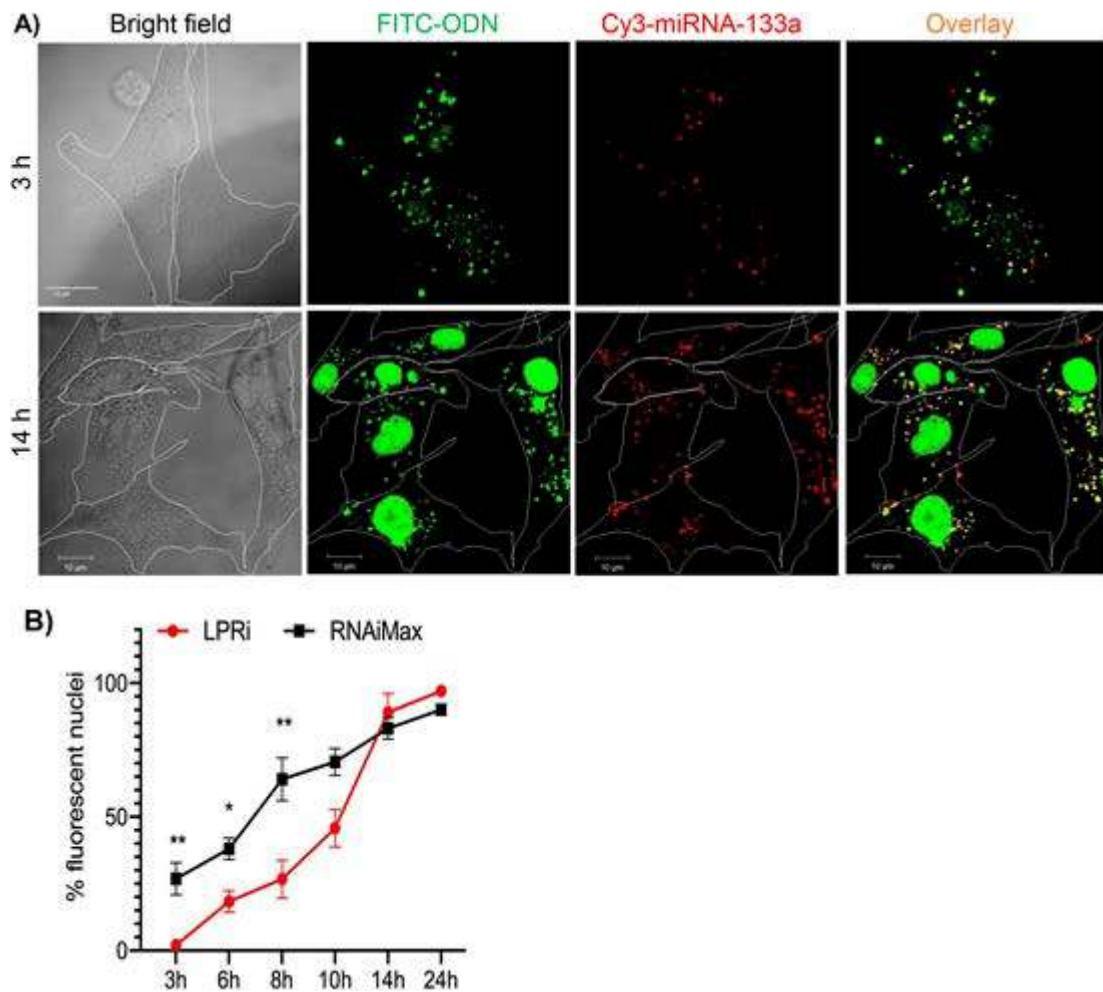


Fig. 3. LPRi and RNAiMax endosomal escape efficiency. A) Fluorescence confocal microscopy analysis of U87MG fixed cells after incubation with LPRi containing an equimolar mixture of Cy3-miRNA-133a and FITC-ODN for 3 and 14 h. B) Endosomal escape efficiency expressed as the percentage of FITC-ODN fluorescent nuclei detected from 15 to 20 images for each time point; one representative of three independent experiments. For all panels, values are mean \pm SEM. * $p < 0.05$, ** $p < 0.01$.

lipin (58% of inhibition) and Genistein (44% of inhibition), two inhibitors of caveolae-mediated endocytosis. Partial inhibition of the luciferase activity was detected when the cells were pre-incubated with cytochalasin D (32% inhibition) and Chlorpromazine (14% inhibition), respectively two inhibitors of micropinocytosis and clathrin-mediated endocytosis pathways (Fig. 4A). In contrast, no significant reduction of luciferase activity was detected when the cells were treated with Chloroquine (100 μ M), an endosomal acidification inhibitor (Supplementary Fig. S3B). When same treatment inhibitors were performed in cells transfected with the RNAiMax, a significant reduction of luciferase activity was detected only when the U87MG LentiRILES/133 T cells were pre-treated with Chlorpromazine (50% inhibition) (Fig. 4A). Then a pulse-chase study (1-h pulse incubation followed by a chase for 15 min up to 6 h) was performed to follow the intracellular fate of Cy3-miRNA-133a in LPRi transfected-U87MG cells. After the indicated time points, the cells were PFA-fixed and slides were analysed by confocal microscopy. As shown in Fig. 4B, C, the Cy3-miRNA-133a largely co-localized with the EGFP-positive Caveolin-1 marker. Kinetic studies indicated that the colocalization of Cy3-miRNA-133a with the Caveolin-1 marker was maximum as early as 15 min post-incubation, decreased over the next 4 h and reached a plateau after 6 h. In contrast, colocalization of FITC-miRNA-133a with RFP-positive Clathrin Light Chain (CLC) was very low from 15 min to 6 h (Fig. 4B, C). These results indicate that LPRi.miRNA-133a complexes were preferentially internalized in the U87MG cells by the caveolin-dependent endocytosis pathway while the RNAiMax.miRNA-133a are more likely internalized in

cells by the clathrin-mediated endocytosis pathway (Fig. 3A). Furthermore, co-localization of Cy3-miRNA-133a with eGFP-Rab5 early endosomes was detected as early as 15 min after incubation with LPRi.miRNA-133a that tended to decrease over the next 6 h (Fig. 4B, C). The co-localization of Cy3-miRNA-133a with eGFP-positive Rab7 late endosomes was low after 15 min of transfection and slightly increased over the next 6 h (Fig. 4B, C). Interestingly, the co-localization of Cy3-miRNA-133a and the eGFP-positive LAMP1 marker of multi vesicular bodies (MVB) and lysosomes was intermediate at 15 min and high after 6 h (Fig. 4B, C). The increased colocalization of miRNAs with Cav-1 and LAMP-1 positive vesicles for prolonged periods of time, in comparison to Rab-5 and Rab-7 endosomal vesicles, prompted us to hypothesize that a fraction of Caveolin-1 positive vesicles might fuse directly with the LAMP-1 positive vesicles. A significant co-localization of RFP-Caveolin-1 with eGFP-LAMP-1 markers was observed after LPRi transfection that tended to increase gradually from 15 min up to 6 h (Fig. 4D). We also observed a triple co-localization of Cy5-miRNA-133a, RFP-positive Caveolin-1 and eGFP-positive LAMP-1 at 4 h post-incubation, suggesting a transport of the miRNA from the caveolae to the MVB/lysosomes (Fig. 4E).

3.5. miRNA processing kinetics and functional implication of P-body proteins

While the mechanisms of nanocarrier internalization in cells are well documented [22–26], less is known about the cytosolic struc-

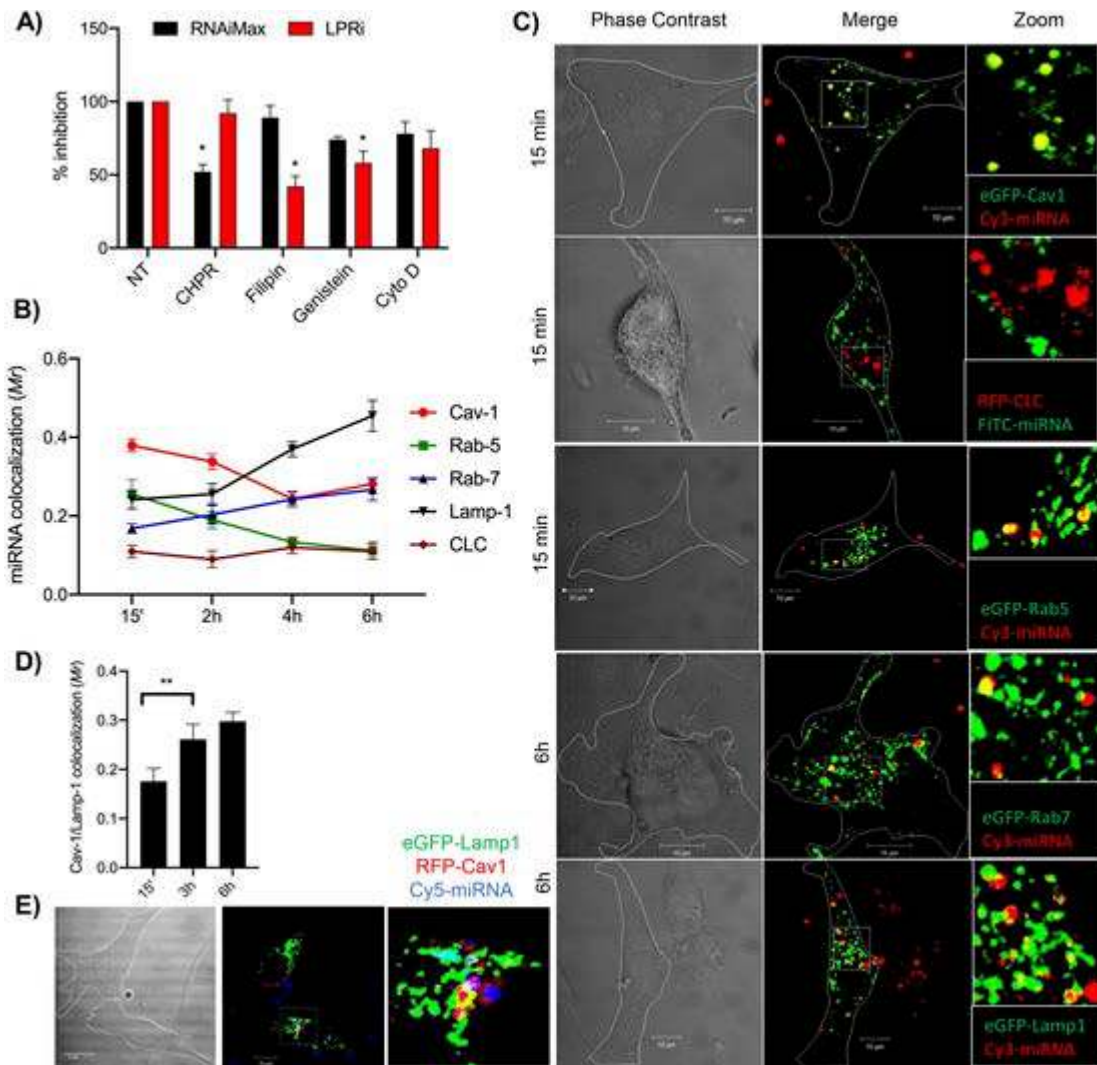


Fig. 4. Intracellular trafficking of miRNA-133a. **A)** U87MG LentiRILES/133 T cells were pre-incubated with specific inhibitors of the caveolae (Filipin and Genistein), clathrin (Chlorpromazine, CHPR) and macropinocytosis (cytochalasin D, Cyto D) internalization pathways before miRNA-133a transfection with LPRi or RNAiMax. Then 48 h later the luciferase activity in cells was quantified ($n = 3$). **B)** U87MG cells expressing eGFP-Cav1, RFP-CLC, eGFP-Rab5, eGFP-Rab7 or eGFP-Lamp1 were transfected for 1 h (pulse) with LPRi.Cy3-miRNA-133a then washed and further incubated for 15 min, 2, 4 or 6 h, fixed in 3% PFA and analysed by confocal microscopy analysis ($n = 4$). **C)** Representative images from eGFP-Cav1, RFP-CLC and eGFP-Rab5 cells collected at a 15-min time point and from eGFP-Rab7 or eGFP-Lamp1 cells collected at a 6-h time points. **D)** Quantification of co-localization events between RFP-Cav1 and eGFP-Lamp1 detected at 15 min, 3 and 6 h post-incubation ($n = 3$). **E)** Co-localization of LPRi.Cy5-miRNA-133a with RFP-Cav1 and eGFP-Lamp1 after 3 h incubation ($n = 3$). For all panels, values are mean \pm SEM; * $p < 0.05$, ** $p < 0.01$; *** $p < 0.001$.

tures where miRNAs are processed by the RISC machinery to exercise their post-transcriptional repressive function. To gain insight into this process, we first studied the co-localization of Cy3-miRNA-133a with FITC-AGO-2 (Fig. 5A), a well-known core catalytic component of the RISC machinery [54]. Throughout our intracellular trafficking experiments, the cells were first incubated with LPRi.Cy3-miRNA-133a for 1 h, washed and further incubated for up to 9 h. Punctate co-localization between miRNA and AGO-2 was low after 15 min incubation with the LPRi.miRNA-133a but increased over the following 9 h (Fig. 5A, B). Similar co-localization kinetics were observed with eGFP-GW182, eGFP-DCP1a and RFP-DDX6, three protein markers of P-bodies [55–61]. To examine whether these proteins participate in the activity of transfected miRNA-133a, we silenced their expression in the U87MG LentiRILES/133 T cells (Supplementary Fig. S5) and evaluated the impact of this silencing process on the luciferase activity. The results indicated that, as expected, AGO-2 silencing decreased the luciferase activity by 66% while the silencing of GW-182 and DDX6 decreased it

by 42% and 34% respectively (Fig. 5C). On the contrary, the silencing of DCP1a had no significant impact on the luciferase activity detected in U87MG LentiRILES/133 T cells. These results suggest that in contrast to AGO-2, GW-182 and DDX6, DCP-1a may not play a functional role in the activity of transfected miRNAs (Fig. 5C). Furthermore, we observed strong co-localization between miRNA-133a and AGO-2 in the first minutes-to-hours of incubation with LPRi.miRNA-133a (Fig. 5B). Thus, we investigated whether AGO-2 might be associated with the membrane of the vesicles containing LPRi.miRNA-133a. Triple co-localization experiments using Cy5-miRNA-133a, FITC-AGO2 and eGFP-Caveolin 1 showed a clear co-localization between these 3 markers (Fig. 5D, left panel). We also observed a triple co-localization between Cy5-miRNA-133a, AGO-2 and LAMP-1 (Fig. 5D, right panel). These results suggest for the first time to our knowledge that AGO-2 might interact with miRNAs inside or at the periphery of these endocytosis vesicles soon after transfection and probably after their delivery in the cytosol.

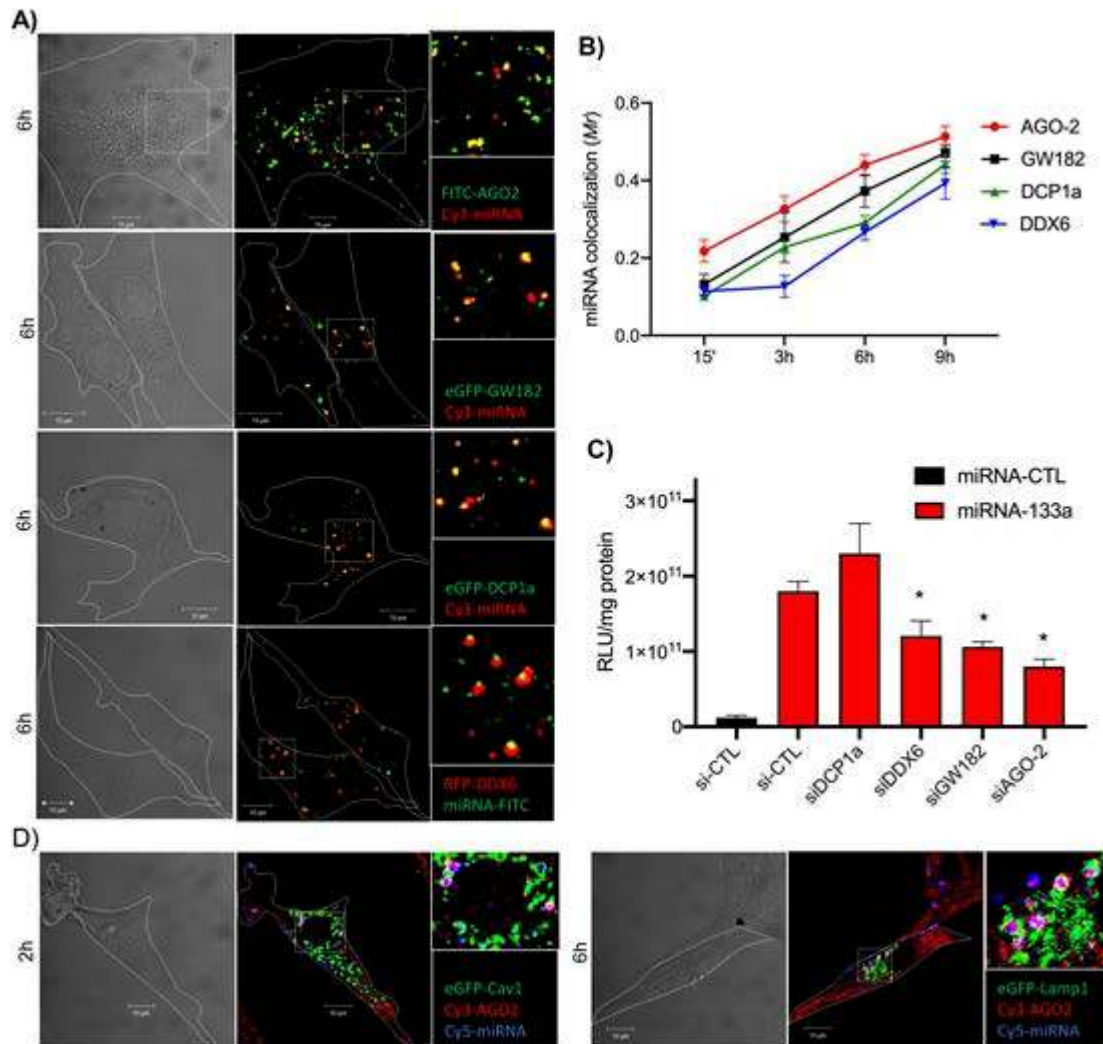


Fig. 5. Functional involvement of Argonaute 2 and P-body markers in miRNA-133a processing after transfection. U87MG cells expressing either eGFP-GW182, eGFP-DCP1a or RFP-DDX6 were incubated for 1 h with LPRI containing miRNA-133a labelled with Cy3 or FITC then washed and further incubated for 15 min, 3, 6 and 9 h, fixed in 3% PFA and analysed by confocal microscopy. In the upper panel cells were also stained with FITC-Ago2 antibody. A) Representative confocal microscopy images and B) quantification of co-localization events between miRNA-133a, AGO-2 and P-body protein markers from 15 to 30 images collected at each time point after the 1-h pulse incubation, in three independent experiments. C) Functional implication of DDX6, GW182, DCP1a and AGO-2 in miRNA-133a processing. The U87MG LentiRILES/133 T cells were transfected with siRNAs specific to DDX6, GW182, DCP1a and AGO-2 and then with the LPRI.miRNA-133a before quantifying the luciferase activity 48 h later ($n = 3$). D) Representative images from three independent experiments of eGFP-Cav1 (left panel) and eGFP-LAMP1 (right panel) positive cells incubated for 2 and 6 h respectively with Cy5-miRNA-133a and stained with Cy3-AGO-2. For all panels, values are mean \pm SEM; * $p < 0.05$, ** $p < 0.01$; *** $p < 0.001$.

3.6. miRNA exocytosis

In long term incubation, we observed that the luciferase activity detected in the U87MG LentiRILES/133 T was maintained over 10 days following a single transfection of LPRI.miRNA-133a (Fig. 6A). We hypothesized that the LPRI-transfected miRNA-133a might be exocytosed into the culture medium and then re-captured by cells, resulting in a long-lasting activity of the RILES/133 T. To address this point, we isolated vesicles from the extracellular medium of LPRI.miRNA-133a-transfected cells and evaluated the presence of miRNA-133a in those vesicles by RT-qPCR. Results of this analysis indicated that the relative expression of miRNA-133a was 158.2 and 291.3 fold higher than that of miRNA-21.5 and -23a respectively, which were used as miRNA house-keeping genes (Fig. 6B). In contrast, expression of this miRNA-133a was barely detected in vesicles collected from cells transfected with the miRNA control (LPRI.miRNA CTL). To determine the subtype of these vesicles, we evaluated their size and shape using a Nano-

sizer and transmission electron microscopy (TEM). As shown in Fig. 6D, E, the collected vesicles exhibited an average size of 138.9 ± 16 nm measured by DLS with a neutral Zeta potential. The TEM analysis revealed spherical vesicles with a similar average size (Fig. 6C). Then, we examined the expression pattern of exosome markers by western-blot. As shown in Fig. 6F, the vesicles were found positive for the presence of the CD63 transmembrane protein as well as TSG101 and ALIX cytosolic proteins and negative for the presence of the GM130 Golgi marker, attesting that these extracellular vesicles were "bona-fide" exosomes [44]. We then incubated the U87MG LentiRILES/133 T cells with conditioned media collected 3 days after transfection of U87MG cells with the LPRI.miRNA-133a or LPRI.miRNA CTL to evaluate whether these vesicles might be capable to re-transfer the miRNA-133a into these cells. As shown in Fig. 6G, the luciferase activity quantified in the U87MG LentiRILES/133 T cells incubated with conditioned media from LPRI.miRNA-133a-transfected cells was 2.5-fold higher than the luciferase activity detected in the same cells but incubated with conditioned media collected from cells transfected with the LPRI.miRNA control.

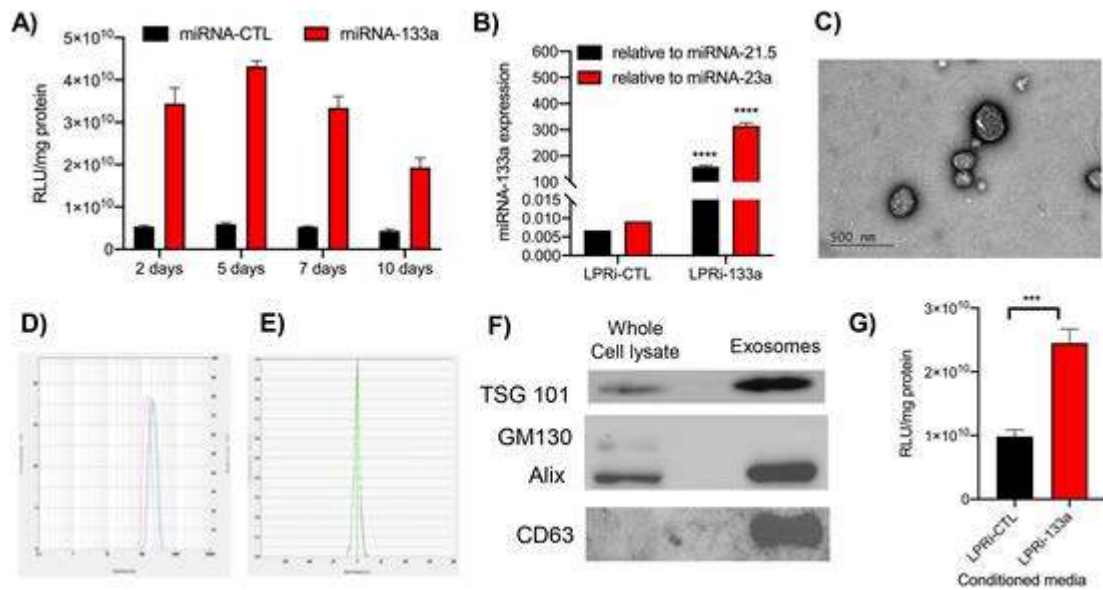


Fig. 6. Implication of extracellular vesicles in the long-term luciferase activity of the U87MG LentiRILES/133 T cells. **A)** The U87MG LentiRILES/133 T cells were transfected once with the LPRi.miRNA-133a and then the luciferase activity was quantified after 5, 7 and 10 days post-transfection ($n = 4$). **B)** RT-qPCR relative expression of miRNA-133a in extracellular vesicles purified from the U87MG cells transfected with the LPRi.miRNA-133a or LPRi-miRNA CTL ($n = 3$). **C)** Morphology, **D)** size and **E)** charge analysis of extracellular vesicles purified from the U87MG cells transfected with the LPRi.miRNA-133a by transmission electron microscopy (**C**) and using a Nanosizer (**D, E**). **F)** Characterization of extracellular vesicles by immunoblotting staining of TSGO1, CD63 and Alix as positive exosome markers and GM130 as negative exosome marker. **G)** Luciferase activity detected in U87MG LentiRILES/133 T cells incubated for 48 h with conditioned media collected from U87MG cells transfected with either LPRi.miRNA-133a or LPRi.miRNA CTL ($n = 4$). For all panels, values are mean \pm SEM. * $p < 0.05$, ** $p < 0.01$; *** $p < 0.001$.

3.7. *In vivo* miRNA-133a delivery with LPRi in LentiRILES/133 T positive glioblastoma tumour

Lastly, we evaluated whether our LPRi lipopolyplexes might be an efficient nanocarrier to deliver miRNA in glioblastoma tumours. For this purpose, we infused glioblastoma tumour with LPRi.miRNA-133a by the convection-enhanced delivery method to closely mimic the clinical situation of the locoregional delivery of drugs [62]. First, the U87MG LentiRILES/133T cells were transduced with lentiviral particles expressing constitutively the Renilla Luciferase (R-Luc) reporter gene to normalize the Firefly luciferase activities (F-Luc) emitted from the RILES/133 T according to each tumour volume. This dual U87MG LentiRILES/133T reporter cell line was then implanted into the right striatum of SCID mice. After 12 days, when mice developed solid brain tumours as assessed by MRI imaging (Fig. 7A), LPRi containing 2 μg of miRNA133a or miRNA CTL in a final volume of 7 μL was infused by CED at a speed of 0.5 $\mu\text{g}/\mu\text{L}$ into the brain of mice. Three days later, the mice were scanned using a bioluminescence scanner. As shown in Fig. 7C, bioluminescence imaging of mice revealed a 3.5-fold higher F-Luc to R-Luc luciferase ratio in the miRNA-133a group of mice as compared to the ratio detected in the miRNA CTL control group of mice, set to the arbitrary ratio value of 1. Quantitative RT-PCR performed at autopsy of mice on the same day confirmed the *in vivo* bioluminescence imaging data. The relative expression of miRNA-133a in the glioblastoma tumour infused with miRNA-133a was 3.2-fold higher than with the miRNA CTL (Fig. 7D).

4. Discussion

Despite the tremendous interest in microRNA therapeutics, their efficient delivery in tumour remains the major obstacle for therapeutic applications [59]. Understanding the behaviours of miRNAs delivered in cells is fundamental to further improve their efficacy. Cationic lipid (lipopolyplexes) and cationic polymer (polyplexes) formulations are the most widely studied RNAi carriers and some of them were recently approved for clinical use [63–66]. In contrast, less is known about ternary lipopolyplexes formulations comprising lipopolyplexes, poly-

plexes and nucleic acids [67]. Our group has designed several lipopolyplexes carriers based on polyplexes made with histidinylated derivatives of polylysine or linear polyethylenimine (His-IPEI, cationic polymers) encapsulated in LIP 100 liposomes formed by *N*-methyl imidazolium lipophosphoramidate (cationic lipid) and histamine lipophosphoramidate (ionizable lipid). We demonstrated the versatility of this lipopolyplexes formulation to transfer pDNA, siRNA and mRNA in different cell types [14–17,45]. More recently, we grafted a tri-mannose antenna on LIP 100 and reported efficient mRNA vaccination against tumour cells after systemic or intradermal administration [15,45]. In an earlier work, we demonstrated that these lipopolyplexes can safely and efficiently deliver siRNA in HeLa cells [14]. However, the exact mechanisms by which these RNAi oligonucleotides were transported inside the cells and how they reached the cytosol to be processed by the RISC machinery was not reported. Here we developed a combined approach using confocal microscopy intracellular studies with our previously described miRNA-ON functional monitoring system [37–39], to comprehensively decipher the mechanisms of miRNA internalization and processing by the RISC machinery in glioblastoma cells. We demonstrated that subcloning the RILES in a lentiviral expression system (LentiRILES) offers the opportunity to monitor in real time and non-invasively the fate of miRNA activity in glioblastoma cells during longitudinal studies performed over several hours to days post-transfection. We show that LPRi is as efficient as the golden standard RNAiMax to transfect the U87MG cells *in vitro* but does not deliver miRNA in the same manner. We investigated the mechanism(s) beyond this dual transfection kinetics and demonstrated that the LPRi.miRNA lipopolyplexes are preferentially internalized in cells through the caveolae-dependent endocytosis pathway followed by trafficking to the endosomal vesicles and multivesicular bodies (MVB), while RNAiMax is more prone to enter cells by clathrin-dependent endocytosis. We also provide evidence that once released into the cytosol, a fraction of detectable miRNA oligonucleotides was captured by Argonaute 2 and trafficked to P-bodies for storage while some miRNAs were secreted to the extracellular medium through exosomes before being re-captured functionally by the cells. We finally proved the effectiveness of our LPRi to deliver miRNA in an ortho-

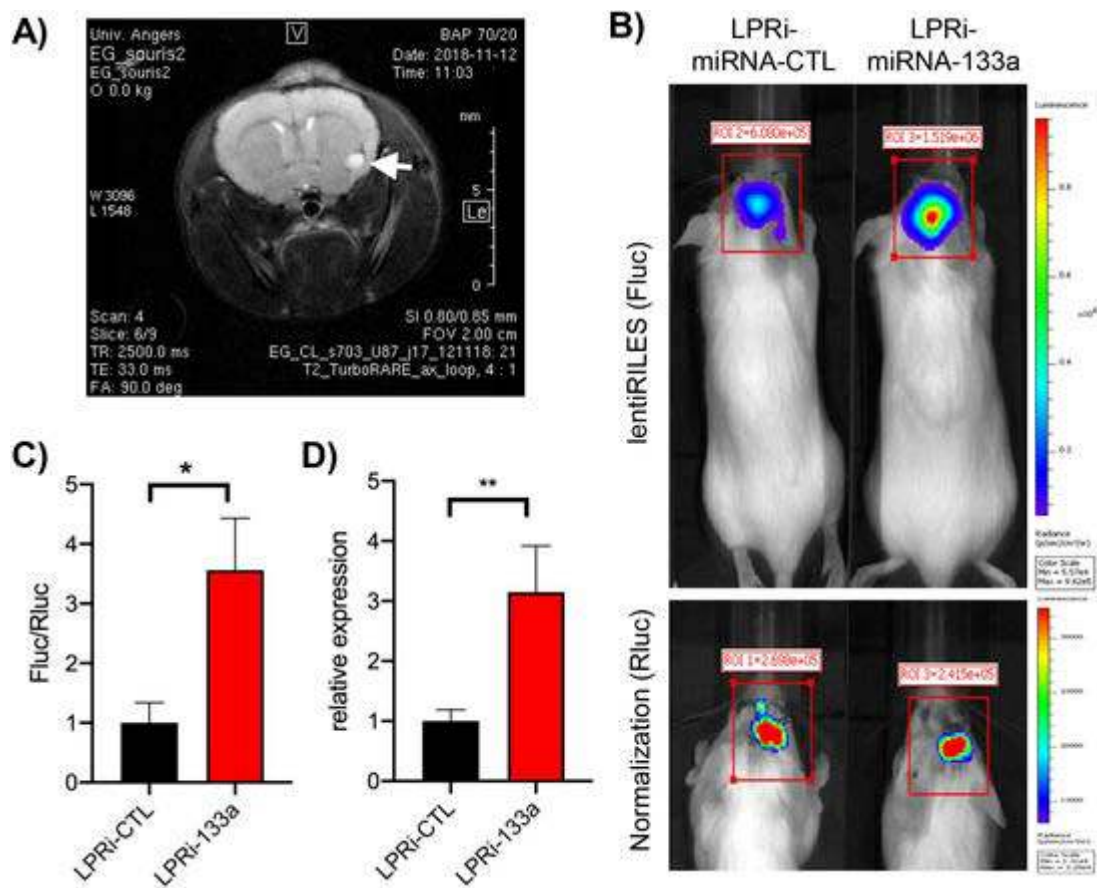


Fig. 7. *In vivo* bioluminescence monitoring of miRNA-133a delivery in the U87MG LentiRILES/133 T cells implanted in the striatum of mice. A) Representative MRI image of tumour mass (arrow) detected in the brain of SCID mice 12 days after implantation of the U87MG LentiRILES/133 T cells. B) Representative dual-bioluminescence imaging of mice collected 3 days after the CED infusion of brain tumours with either LPRi.miRNA-133a ($n = 5$ mice) or LPRi.miRNA CTL ($n = 5$ mice). To normalize activity of the RILES/133 T in tumours according to tumour masses, the mice were first injected with Luciferin substrate to monitor activities of the Firefly Luciferase (FLuc, *Top panel*) and then 6 h later with the coelenterazin substrates to monitor activities of the Renilla luciferase (RLuc, *Lower panel*) C) Quantification of bioluminescence signals emitted from brain tumours as in (B) and expressed as ratio of FLuc-to-RLuc. D) RT-qPCR relative expression of miRNA-133a in brain tumours from (B, C) collected at autopsy of mice immediately after the *in vivo* bioluminescence imaging. For all panels, values are mean \pm SEM. * $p < 0.05$, ** $p < 0.01$, *** $p < 0.001$.

topic human to mouse animal model of glioblastoma by CED infusion of tumour mass with LPRi.miRNA-133a.

A major point of interest in our intracellular trafficking investigations is that we uncovered the mechanism(s) responsible for the time shift delay in miRNA activity detected in U87MG LentiRILES/133T following transfection with LPRi.miRNA-133a (Fig. 1). We demonstrated that the endosomal escape of LPRi.miRNA-133a occurred at a later time point compared to the endosomal escape performed by RNAiMax.miRNA-133a (Fig. 3). Using specific pharmacological endocytosis inhibitors and confocal microscopy analysis of cells expressing fluorescent subcellular markers, we revealed that LPRi use the caveolae pathway as the main route of internalization in U87MG cells (Fig. 4). Caveolae are lipid raft-enriched, bulb-shaped plasma membrane structures that traffic internalized molecules to endosomes. Early [68,69] and more recent studies [70–72] reported that cell surface caveolae exhibit limited motility and dynamics compared to the mobility of vesicles derived from the clathrin-endocytosis pathway. Previous experimental evidence indicated that the Lipofectamine-based reagents such as RNAiMax enter the cells preferentially by this fast-motion clathrin-endocytosis pathway [73,74]. Our results in Fig. 4A corroborated these data as we found that the Clathrin inhibitor significantly blocks the activity of miRNA when transfected with the RNAiMax transfection reagent. Therefore, the difference in the internalization routes used by these two transfection reagents might explain in part the different kinetics observed for endosomal escape study and miRNA activity detected by the RILES at early time points post-transfection. Trafficking

of LPRi through the caveolae pathway might therefore appear to be counterproductive and a disadvantage for miRNA delivery. However, studies indicated that native macromolecules as well as various pathogens preferentially enter cells through caveolae, presumably to prevent lysosome degradation [75,76]. Other studies demonstrated that targeting the caveolae pathway is an efficient strategy for the successful delivery of cargo due to its slow acidification process after fusion with acidified vesicles. For example, glycopolymer-based carriers enter cells through different routes while only caveolae-mediated endocytosis leads to efficient transfection [77,78]. Histone-targeted polyplexes enter cells by the caveolae for efficient delivery of plasmid DNA to the nucleus [79]. Furthermore, the overexpression of Caveolin-1 in inflammatory breast cancer cells has been shown to increase the transfection efficiency of histone-targeted polyplexes [67]. Although we do not provide here the explanation why the LPRi are preferentially taken up by Caveolin-dependent endocytosis, it is likely that the chemical composition and structure of LPRi might be responsible for this. In a previous study we showed that plasmid DNA loaded-lipopolyplexes use the same Caveolin-dependent endocytosis pathway to deliver pDNA in C2C12 cells [28]. It is documented that the uptake of nucleic acids is dependent on the nature of the nanocarriers [80]. For instance, lipoplexes containing the cationic lipid DOTAP are exclusively internalized by a clathrin-dependent endocytosis pathway, while polyplexes prepared from the cationic polymer polyethyleneimine (PEI) were internalized by both the clathrin- and caveolin- endocytosis pathways [77].

Following endosomal/MVB escape, miRNAs are released in the cytosol where they enter the RISC machinery to exercise their repressive post-transcriptional activity [22]. We provide evidence that once in the cytosol, a fraction of miRNA-133a is captured by Argonaute-2 and trafficked to P-bodies. We detected intense cytosolic localisation of the fluorescent miRNA-133a with P-body markers such as GW182, DDX6 and DCP1a (Fig. 5A and Supplementary Table S1). The fraction of transfected miRNA-133a free to diffuse in the cytosol cannot be visualized by standard confocal fluorescent microscopy. Sophisticated fluorescent microscopy equipment and/or labelling strategies are required for that purpose [22,27,81–83]. Nevertheless, we show that miRNAs are routed to P-bodies in a gradual manner over time, from 3 to 9 h post incubation with LPRI.miRNA-133a. The silencing of the expression of AGO2 and P-body markers in U87MG LentiRILES/133T before transfection with LPRI.miRNA-133a resulted in a reduced luciferase activity of the RILES/133T system upon AGO2, GW182 and DDX6 silencing but not upon DCP-1a silencing (Fig. 5C). This indicates that DCP1a - a more specific marker of P-bodies [30,84,85] is unlikely to play a functional role in the transcriptional repressive activity of delivered miRNAs. The exact role of P-bodies in miRNA processing is not fully understood and still under debate [86–88]. However, two recent reports shed light on the roles of P-bodies in miRNA and mRNA processing. Using a novel fluorescence-activated particle sorting (FAPS) approach to purify cytosolic P-bodies, Hubstenberger et al. [58] showed that mRNAs segregated into P-bodies are not processed for decay/degradation but rather stored in a coordinated manner providing as such a reservoir that can be mobilized to adapt protein production to cellular needs. More recently, Pitchiaya et al. [85] followed the dynamic localization of individual miRNAs, mRNAs and long non-coding RNA to P-bodies using intracellular single-molecule fluorescence microscopy. They revealed that unused miRNAs stably bind to P-bodies, whereas functional miRNAs, repressed mRNAs, and lncRNAs both transiently and stably localize within either the core or periphery of P-bodies. Our results are in line with these studies. As observed by others [89,90], the amount of miRNA delivered by transfection is far superior to the amount of endogenously expressed miRNAs in cells. It is therefore tempting to suggest that accumulated miRNAs detected in P-bodies of U87MG post-transfection might represent the excess of miRNAs that are not processed by the Ago2/RISC machinery. Thus, they could be transiently stored in these membrane-less foci up to the time that the cytosolic RISC machinery becomes again available. In the meantime, it remains unclear how miRNAs are transported to P-bodies to be transiently stored.

In this specific context, several studies suggested that in addition to the diffuse form of AGO-2 within the cytosol, AGO-2 is also enriched on the cytoplasmic side of endosomes [91–93]. Based on these findings, we hypothesized that the detected presence of AGO-2 in caveolae and MVB of U87MG might facilitate the capture of transfected miRNAs by Argonaute 2. Triple co-localization studies revealed, for the first time to our knowledge, that transfected miRNA-133a co-localized with AGO-2 and at the same time with Caveolin-1 as soon as 2 h post incubation with the LPRI as well as with Lamp-1 vesicles after 6 h of incubation. It could be hypothesized that miRNAs inside caveolae and MVBs (alternatively early and late endosomal vesicles as well) could be captured by AGO-2 immediately after their endosomal escape and processed by the RISC machinery and/or trafficked to P-bodies for transient storage.

Another intriguing aspect of our finding is that the RILES miRNA monitoring system remained switched-ON over a long period of time in the U87MG LentiRILES/133T after a single transfection of miRNA-133a. Exocytosis of transfected miRNAs has been reported to be responsible for prolonged transfection efficiency if the exocytosed complexes are internalized again and processed efficiently by the RISC [25,26,94,95]. Here we demonstrated that a fraction of transfected miRNA-133a is detectable in vesicle-apparent exosomes and that

the conditioned medium collected from miRNA-133a-transfected U87MG cells is sufficient to activate the RILES/133T in the non-transfected U87MG LentiRILES/133T cells (Fig. 6). We have therefore provided a reliable explanation for the long-lasting activation of the LentiRILES/133T in the U87MG (Fig. 6A). However, it cannot be excluded that other extracellular vesicles, different from exosomes, also participate as we invariably observed by TEM several vesicles larger than 200 nm (data not shown).

Finally, we evaluated the potency of our miRNA-lipopolyplexes formulation to deliver miRNAs in glioblastoma tumour mass. To be closer to clinical practice, we employed the CED method to deliver miRNA lipopolyplexes locoregionally in the U87MG LentiRILES/133T glioblastoma tumour mass. Bioluminescence *in vivo* imaging of the luciferase activity of the RILES/133T in these tumours enabled us to provide experimental evidence that LPRI can deliver active miRNA-133a in glioblastoma. A 3.5-fold induction of luciferase activity in tumour mass was measured as compared to infused LPRI containing the miRNA control. This result was confirmed by qRT-PCR performed in tumours after autopsy of the mice (Fig. 7). These data prove that CED infusion of LPRI.miRNA-133a results in an adequate delivery of miRNAs in tumour mass followed by efficient uptake by tumour cells and processing by the RISC machinery. We are currently exploiting the RILES/133T monitoring system to establish the exact kinetics of miRNA activity in mice upon delivery of LPRI.miRNA-133a in a bioluminescence longitudinal study. Our objective is to tailor a protocol (dosing, injection time, and schedule) to administer a therapeutic miRNA with reduced toxicity. Several miRNAs have been identified as tumour suppressors specific to glioblastoma such as miRNA-128, miRNA-34a, miRNA-124 or miRNA-137 [96]. We expect a long-lasting effect of the therapeutic miRNA mediated in part by exosomes loaded with the therapeutic miRNAs upon the locoregional delivery using the LPRI.

5. Conclusion

Altogether, our work provides a detailed overview of the mechanisms of internalization, endosomal escape, intracellular trafficking and processing of LPRI-transfected miRNA by the RISC machinery as well as secretion of exosomes into the extracellular space. We provide evidence that LPRI is a suitable formulation to deliver miRNA *in vitro* and *in vivo* in glioblastoma cells and holds promise for glioblastoma treatment.

Funding

This work was supported by the Institut National du Cancer (INCa) [Marengo PLBIO 2014-168 to P.B and E.G]; La Ligue Contre le Cancer [Région du Loiret 2017–2019 to P.B and 2015-2017 to P.M]; ARD 2020 Biopharmaceutics [RNA cell factory 2017–2020 to C.P]; APR-IR Région CVL [VACARME 2017–2018 to C.P].

Uncited references

[97–101]

CRediT authorship contribution statement

Viorel Simion: Conceptualization, Investigation, Validation, Visualization, Writing - original draft, Writing - review & editing. **Elodie Henri:** Investigation. **Viktorija Juric:** Investigation. **Ruth Aquino:** Investigation. **Claire Loussouarn:** Investigation. **Yoan Laurent:** Investigation. **Francisco Martin:** Methodology, Resources. **Patrick Midoux:** Methodology, Resources, Validation, Writing - original draft, Writing - review & editing. **Emmanuel Garcion:** Funding acquisition, Methodology, Resources, Conceptualization. **Chantal Pichon:** Methodology, Resources, Writing - original draft, Writing - review & editing, Conceptualization. **Patrick Baril:** Conceptualization, Funding acquisition, Methodology, Resources, Supervision, Validation, Visualization, Writing - original draft, Writing - review & editing.

Declaration of Competing Interest

Francisco Martin is the inventor of “Highly inducible dual-promoter lentiviral Tet-On (CT/EP2012/059408)” licensed to Canvax Biotech.

Acknowledgement

We thank Stéphanie Lerondel, Maryline Le Mée, Stéphanie Rétif and Julien Sobilo (TAAM/CIPA, CNRS UPS 44, Orléans) for their technical assistance and for access to the Lumina Bioluminescence scanner. We would also like to thank Frederic Fourcher (CBM, CNRS UPR4301, Orléans) and Audrey Sauldubois (Plateforme Régionale de Microscopie Electronique, Université d'Orléans, France) for their support and analysis of the AFM and TEM images. We finally thank Elizabeth Rowley-Jolivet (elizabeth.rowley-jolivet@orange.fr) for English language editing.

Appendix A. Supplementary data

Supplementary data to this article can be found online at <https://doi.org/10.1016/j.jconrel.2020.08.028>.

References

- [1] R C Lee, R L Feinbaum, V Ambros, The *C. elegans* heterochronic gene *lin-4* encodes small RNAs with antisense complementarity to *lin-14*, *Cell* 75 (5) (1993) 843–854.
- [2] A Kozomara, S Griffiths-Jones, miRBase: annotating high confidence microRNAs using deep sequencing data, *Nucleic Acids Res.* 42 (Database issue) (2014) D68–D73.
- [3] D P Bartel, MicroRNAs: target recognition and regulatory functions, *Cell* 136 (2) (2009) 215–233.
- [4] Z Li, T M Rana, Therapeutic targeting of microRNAs: current status and future challenges, *Nat. Rev. Drug Discov.* 13 (8) (2014) 622–638.
- [5] D Rosenblum, et al., Progress and challenges towards targeted delivery of cancer therapeutics, *Nat. Commun.* 9 (1) (2018) 1410.
- [6] Y Zhang, Z Wang, R A Gemeinhart, Progress in microRNA delivery, *J. Control. Release* 172 (3) (2013) 962–974.
- [7] O S Thomas, W Weber, Overcoming physiological barriers to nanoparticle delivery—are we there yet?, *Front. Bioeng. Biotechnol.* 7 (2019) 415.
- [8] A Shea, et al., MicroRNAs in glioblastoma multiforme pathogenesis and therapeutics, *Cancer Med.* 5 (8) (2016) 1917–1946.
- [9] C A Stine, J M Munson, Convection-enhanced delivery: connection to and impact of interstitial fluid flow, *Front. Oncol.* 9 (2019) 966.
- [10] A Woehrer, L Bauchet, J S Barnholtz-Sloan, Glioblastoma survival: has it improved? Evidence from population-based studies, *Curr. Opin. Neurol.* 27 (6) (2014) 666–674.
- [11] P Ofek, et al., Restoring the oncosuppressor activity of microRNA-34a in glioblastoma using a polyglycerol-based polyplex, *Nanomedicine* 12 (7) (2016) 2201–2214.
- [12] N Babae, et al., Systemic miRNA-7 delivery inhibits tumor angiogenesis and growth in murine xenograft glioblastoma, *Oncotarget* 5 (16) (2014) 6687–6700.
- [13] Y P Yang, et al., Inhibition of cancer stem cell-like properties and reduced chemoradioresistance of glioblastoma using microRNA145 with cationic polyurethane-short branch PEI, *Biomaterials* 33 (5) (2012) 1462–1476.
- [14] C Goncalves, et al., Lipopolyplexes comprising imidazole/imidazolium lipophosphoramidate, histidinylated polyethyleneimine and siRNA as efficient formulation for siRNA transfection, *Int. J. Pharm.* 460 (1–2) (2014) 264–272.
- [15] K Van der Jeught, et al., Dendritic cell targeting mRNA lipopolyplexes combine strong antitumor T-cell immunity with improved inflammatory safety, *ACS Nano* 12 (10) (2018) 9815–9829.
- [16] F Perche, et al., Enhancement of dendritic cells transfection *in vivo* and of vaccination against B16F10 melanoma with mannosylated histidinylated lipopolyplexes loaded with tumor antigen messenger RNA, *Nanomedicine* 7 (4) (2011) 445–453.
- [17] F Perche, et al., Gene transfer by histidinylated lipopolyplexes: a dehydration method allowing preservation of their physicochemical parameters and transfection efficiency, *Int. J. Pharm.* 423 (1) (2012) 144–150.
- [18] P Wang, et al., RNA-based therapy for osteogenesis, *Int. J. Pharm.* 569 (2019) 118594.
- [19] P Midoux, et al., Chemical vectors for gene delivery: a current review on polymers, peptides and lipids containing histidine or imidazole as nucleic acids carriers, *Br. J. Pharmacol.* 157 (2) (2009) 166–178.
- [20] O Boussif, et al., A versatile vector for gene and oligonucleotide transfer into cells in culture and *in vivo*: polyethylenimine, *Proc. Natl. Acad. Sci. U. S. A.* 92 (16) (1995) 7297–7301.
- [21] Z ur Rehman, D Hoekstra, I S Zuhorn, Mechanism of polyplex- and lipoplex-mediated delivery of nucleic acids: real-time visualization of transient membrane destabilization without endosomal lysis, *ACS Nano* 7 (5) (2013) 3767–3777.
- [22] J Gilleron, et al., Image-based analysis of lipid nanoparticle-mediated siRNA delivery, intracellular trafficking and endosomal escape, *Nat. Biotechnol.* 31 (7) (2013) 638–646.
- [23] M Lazebnik, R K Keswani, D W Pack, Endocytic transport of polyplex and lipoplex siRNA vectors in HeLa cells, *Pharm. Res.* 33 (12) (2016) 2999–3011.
- [24] A Wittrup, et al., Visualizing lipid-formulated siRNA release from endosomes and target gene knockdown, *Nat. Biotechnol.* 33 (8) (2015) 870–876.
- [25] G Sahay, et al., Efficiency of siRNA delivery by lipid nanoparticles is limited by endocytic recycling, *Nat. Biotechnol.* 31 (7) (2013) 653–658.
- [26] R S Shukla, et al., Intracellular trafficking and exocytosis of a multi-component siRNA nanocomplex, *Nanomedicine* 12 (5) (2016) 1323–1334.
- [27] H C Luo, et al., Comparison of the cellular transport mechanism of cationic, star-shaped polymers and liposomes in HaCat cells, *Int. J. Nanomedicine* 12 (2017) 1085–1096.
- [28] L Billiet, et al., Gene transfer by chemical vectors, and endocytosis routes of polyplexes, lipoplexes and lipopolyplexes in a myoblast cell line, *Biomaterials* 33 (10) (2012) 2980–2990.
- [29] V Capel, et al., Insight into the relationship between the cell culture model, cell trafficking and siRNA silencing efficiency, *Biochem. Biophys. Res. Commun.* 477 (2) (2016) 260–265.
- [30] J Liu, et al., MicroRNA-dependent localization of targeted mRNAs to mammalian P-bodies, *Nat. Cell Biol.* 7 (7) (2005) 719–723.
- [31] A Jagannath, M J Wood, Localization of double-stranded small interfering RNA to cytoplasmic processing bodies is Ago2 dependent and results in up-regulation of GW182 and Argonaute-2, *Mol. Biol. Cell* 20 (1) (2009) 521–529.
- [32] S P Chan, F J Slack, microRNA-mediated silencing inside P-bodies, *RNA Biol.* 3 (3) (2006) 97–100.
- [33] A Jakymiw, et al., Disruption of GW bodies impairs mammalian RNA interference, *Nat. Cell Biol.* 7 (12) (2005) 1267–1274.
- [34] C Y Chu, T M Rana, Translation repression in human cells by microRNA-induced gene silencing requires RCK/p54, *PLoS Biol.* 4 (7) (2006) e210.
- [35] A Eulalio, I Behm-Ansmant, E Izaurralde, P bodies: at the crossroads of post-transcriptional pathways, *Nat. Rev. Mol. Cell Biol.* 8 (1) (2007) 9–22.
- [36] A Eulalio, et al., P-body formation is a consequence, not the cause, of RNA-mediated gene silencing, *Mol. Cell Biol.* 27 (11) (2007) 3970–3981.
- [37] S Ezzine, et al., RILES, a novel method for temporal analysis of the *in vivo* regulation of miRNA expression, *Nucleic Acids Res.* 41 (20) (2013) e192.
- [38] V Simion, et al., Positive radionuclide imaging of miRNA expression using RILES and the human sodium iodide symporter as reporter gene is feasible and supports a protective role of miRNA-23a in response to muscular atrophy, *PLoS One* 12 (5) (2017) e0177492.
- [39] P Baril, C Pichon, Positive bioluminescence imaging of microRNA expression in small animal models using an engineered genetic-switch expression system, *RILES, Methods Mol. Biol.* 1372 (2016) 193–208.
- [40] M Mevel, et al., Synthesis and transfection activity of new cationic phosphoramidate lipids: high efficiency of an imidazolium derivative, *Chembiochem* 9 (9) (2008) 1462–1471.
- [41] M Mevel, et al., Novel neutral imidazole-lipophosphoramidates for transfection assays, *Chem. Commun. (Camb.)* (27) (2008) 3124–3126.
- [42] F Perche, et al., Selective gene delivery in dendritic cells with mannosylated and histidinylated lipopolyplexes, *J. Drug Target.* 19 (5) (2011) 315–325.
- [43] K Benabdellah, et al., Development of an all-in-one lentiviral vector system based on the original TetR for the easy generation of Tet-ON cell lines, *PLoS One* 6 (8) (2011) e23734.
- [44] C Thery, et al., Minimal information for studies of extracellular vesicles 2018 (MISEV2018): a position statement of the International Society for Extracellular Vesicles and update of the MISEV2014 guidelines, *J. Extracell. Vesicles* 7 (1) (2018) 1535750.
- [45] A Le Moignic, et al., Preclinical evaluation of mRNA trimannosylated lipopolyplexes as therapeutic cancer vaccines targeting dendritic cells, *J. Control. Release* 278 (2018) 110–121.
- [46] L G Rikkert, et al., Quality of extracellular vesicle images by transmission electron microscopy is operator and protocol dependent, *J. Extracell. Vesicles* 8 (1) (2019) 1555419.
- [47] D Sehedic, et al., Locoregional confinement and major clinical benefit of (188)re-loaded CXCR4-targeted nanocarriers in an orthotopic human to mouse model of glioblastoma, *Theranostics* 7 (18) (2017) 4517–4536.
- [48] A T Das, L Tenenbaum, B Berkhout, Tet-on systems for doxycycline-inducible gene expression, *Curr. Gene Ther.* 16 (3) (2016) 156–167.
- [49] A Nishiyama, R Suzuki, X Zhu, NG2 cells (polydendrocytes) in brain physiology and repair, *Front. Neurosci.* 8 (2014) 133.
- [50] F Perche, et al., Neutral lipopolyplexes for *in vivo* delivery of conventional and replicative RNA vaccine, *Mol. Ther. Nucleic Acids* 17 (2019) 767–775.
- [51] C Wang, et al., Entry of PIP3-containing polyplexes into MDCK epithelial cells by local apical-basal polarity reversal, *Sci. Rep.* 6 (2016) 21436.
- [52] Q Hu, M B Bally, T D Madden, Subcellular trafficking of antisense oligonucleotides and down-regulation of bcl-2 gene expression in human melanoma cells using a fusogenic liposome delivery system, *Nucleic Acids Res.* 30 (16) (2002) 3632–3641.
- [53] L Y Chou, K Ming, W C Chan, Strategies for the intracellular delivery of nanoparticles, *Chem. Soc. Rev.* 40 (1) (2011) 233–245.
- [54] E Maniataki, Z Mourelatos, A human, ATP-independent, RISC assembly machine fueled by pre-miRNA, *Genes Dev.* 19 (24) (2005) 2979–2990.
- [55] Y Luo, Z Na, S A Slavoff, P-bodies: composition, properties, and functions, *Biochemistry* 57 (17) (2018) 2424–2431.
- [56] R Parker, U Sheth, P bodies and the control of mRNA translation and degradation, *Mol. Cell* 25 (5) (2007) 635–646.

- [57] J Ayache, et al., P-body assembly requires DDX6 repression complexes rather than decay or Ataxin2/2L complexes, *Mol. Biol. Cell* 26 (14) (2015) 2579–2595.
- [58] A Hubstenberger, et al., P-body purification reveals the condensation of repressed mRNA regulons, *Mol. Cell* 68 (1) (2017) 144–157 e5.
- [59] E Seto, et al., The assembly of EDC4 and Dcp1a into processing bodies is critical for the translational regulation of IL-6, *PLoS One* 10 (5) (2015) e0123223.
- [60] A Aizer, et al., Quantifying mRNA targeting to P-bodies in living human cells reveals their dual role in mRNA decay and storage, *J. Cell Sci.* 127 (Pt 20) (2014) 4443–4456.
- [61] D Teixeira, et al., Processing bodies require RNA for assembly and contain nontranslating mRNAs, *RNA* 11 (4) (2005) 371–382.
- [62] W Debinski, S B Tatter, Convection-enhanced delivery for the treatment of brain tumors, *Expert. Rev. Neurother.* 9 (10) (2009) 1519–1527.
- [63] L J Scott, Givosiran: first approval, *Drugs* 80 (3) (2020) 335–339.
- [64] X Zhang, V Goel, G J Robbie, Pharmacokinetics of patisiran, the first approved RNA interference therapy in patients with hereditary transthyretin-mediated amyloidosis, *J. Clin. Pharmacol.* (2019).
- [65] S M Hoy, Patisiran: first global approval, *Drugs* 78 (15) (2018) 1625–1631.
- [66] K Fitzgerald, et al., A highly durable RNAi therapeutic inhibitor of PCSK9, *N. Engl. J. Med.* 376 (1) (2017) 41–51.
- [67] M Rezaee, et al., Progress in the development of lipopolyplexes as efficient non-viral gene delivery systems, *J. Control. Release* 236 (2016) 1–14.
- [68] P Thomsen, et al., Caveolae are highly immobile plasma membrane microdomains, which are not involved in constitutive endocytic trafficking, *Mol. Biol. Cell* 13 (1) (2002) 238–250.
- [69] A Fittipaldi, et al., Cell membrane lipid rafts mediate caveolar endocytosis of HIV-1 Tat fusion proteins, *J. Biol. Chem.* 278 (36) (2003) 34141–34149.
- [70] E Shvets, et al., Dynamic caveolae exclude bulk membrane proteins and are required for sorting of excess glycosphingolipids, *Nat. Commun.* 6 (2015) 6867.
- [71] R G Parton, V A Tilly, B M Collins, Caveolae, *Curr. Biol.* 28 (8) (2018) R402–R405.
- [72] C G Hansen, B J Nichols, Exploring the caves: cavins, caveolins and caveolae, *Trends Cell Biol.* 20 (4) (2010) 177–186.
- [73] F Cardarelli, et al., The intracellular trafficking mechanism of Lipofectamine-based transfection reagents and its implication for gene delivery, *Sci. Rep.* 6 (2016) 25879.
- [74] S Cui, et al., Transmembrane routes of cationic liposome-mediated gene delivery using human throat epidermis cancer cells, *Biotechnol. Lett.* 36 (1) (2014) 1–7.
- [75] A L Kiss, E Botos, Endocytosis via caveolae: alternative pathway with distinct cellular compartments to avoid lysosomal degradation?, *J. Cell. Mol. Med.* 13 (7) (2009) 1228–1237.
- [76] G Sahay, D Y Alakhova, A V Kabanov, Endocytosis of nanomedicines, *J. Control. Release* 145 (3) (2010) 182–195.
- [77] P M McLendon, K M Fichter, T M Reineke, Poly(glycoamidoamine) vehicles promote pDNA uptake through multiple routes and efficient gene expression via caveolae-mediated endocytosis, *Mol. Pharm.* 7 (3) (2010) 738–750.
- [78] N P Gabrielson, D W Pack, Efficient polyethylenimine-mediated gene delivery proceeds via a caveolar pathway in HeLa cells, *J. Control. Release* 136 (1) (2009) 54–61.
- [79] N L Ross, et al., Histone-targeted polyplexes avoid endosomal escape and enter the nucleus during postmitotic redistribution of ER membranes, *Mol. Ther. Nucleic Acids* 4 (2015) e226.
- [80] H Abumanhal-Masarweh, et al., Tailoring the lipid composition of nanoparticles modulates their cellular uptake and affects the viability of triple negative breast cancer cells, *J. Control. Release* 307 (2019) 331–341.
- [81] H Du Rietz, et al., Imaging small molecule-induced endosomal escape of siRNA, *Nat. Commun.* 11 (1) (2020) 1809.
- [82] A Lacroix, et al., Uptake and fate of fluorescently labeled DNA nanostructures in cellular environments: a cautionary tale, *ACS Cent. Sci.* 5 (5) (2019) 882–891.
- [83] R L Juliano, Intracellular trafficking and endosomal release of oligonucleotides: what we know and what we don't, *Nucleic Acid Ther.* 28 (3) (2018) 166–177.
- [84] H Zhou, et al., Residues that affect human Argonaute2 concentration in cytoplasmic processing bodies, *Biochem. Biophys. Res. Commun.* 378 (3) (2009) 620–624.
- [85] S Pitchiaya, et al., Dynamic recruitment of single RNAs to processing bodies depends on RNA functionality, *Mol. Cell* 74 (3) (2019) 521–533 e6.
- [86] A Eulalio, et al., African swine fever virus p37 structural protein is localized in nuclear foci containing the viral DNA at early post-infection times, *Virus Res.* 130 (1–2) (2007) 18–27.
- [87] A R Guzikowski, Y S Chen, B M Zid, Stress-induced mRNP granules: form and function of processing bodies and stress granules, *Wiley Interdiscip. Rev. RNA* 10 (3) (2019) e1524.
- [88] N Standart, D Weil, P-bodies: cytosolic droplets for coordinated mRNA storage, *Trends Genet.* 34 (8) (2018) 612–626.
- [89] H Y Jin, et al., Transfection of microRNA mimics should be used with caution, *Front. Genet.* 6 (2015) 340.
- [90] O Flores, et al., Differential RISC association of endogenous human microRNAs predicts their inhibitory potential, *Nucleic Acids Res.* 42 (7) (2014) 4629–4639.
- [91] Y S Lee, et al., Silencing by small RNAs is linked to endosomal trafficking, *Nat. Cell Biol.* 11 (9) (2009) 1150–1156.
- [92] D J Gibbins, et al., Multivesicular bodies associate with components of miRNA effector complexes and modulate miRNA activity, *Nat. Cell Biol.* 11 (9) (2009) 1143–1149.
- [93] A Antoniou, et al., PICK1 links Argonaute 2 to endosomes in neuronal dendrites and regulates miRNA activity, *EMBO Rep.* 15 (5) (2014) 548–556.
- [94] L Ding, et al., Intracellular fate of nanoparticles with polydopamine surface engineering and a novel strategy for exocytosis-inhibiting, lysosome impairment-based cancer therapy, *Nano Lett.* 17 (11) (2017) 6790–6801.
- [95] S Muro, et al., ICAM-1 recycling in endothelial cells: a novel pathway for sustained intracellular delivery and prolonged effects of drugs, *Blood* 105 (2) (2005) 650–658.
- [96] B Banelli, et al., MicroRNA in glioblastoma: an overview, *Int. J. Genomics* 2017 (2017) 7639084.
- [97] A K Leung, P A Sharp, Quantifying Argonaute proteins in and out of GW/P-bodies: implications in microRNA activities, *Adv. Exp. Med. Biol.* 768 (2013) 165–182.
- [98] A Jakymiw, et al., The role of GW/P-bodies in RNA processing and silencing, *J. Cell Sci.* 120 (Pt 8) (2007) 1317–1323.
- [99] J Liu, et al., A role for the P-body component GW182 in microRNA function, *Nat. Cell Biol.* 7 (12) (2005) 1261–1266.
- [100] M Ernoult-Lange, et al., Multiple binding of repressed mRNAs by the P-body protein Rck/p54, *RNA* 18 (9) (2012) 1702–1715.
- [101] K Rzeczkowski, et al., C-Jun N-terminal kinase phosphorylates DCP1a to control formation of P bodies, *J. Cell Biol.* 194 (4) (2011) 581–596.